

# Innate immune cell response to host-parasite interaction in a human intestinal tissue microphysiological system

Mouhita Humayun<sup>1</sup>, Jose M. Ayuso<sup>2,3,4</sup>, Keon Young Park<sup>5,6</sup>†, Bruno Martorelli Di Genova<sup>7</sup>‡, Melissa C. Skala<sup>1,3</sup>, Sheena C. Kerr<sup>2,6\*</sup>, Laura J. Knoll<sup>7,6\*</sup>, David J. Beebe<sup>1,2,6\*</sup>

Protozoan parasites that infect humans are widespread and lead to varied clinical manifestations, including life-threatening illnesses in immunocompromised individuals. Animal models have provided insight into innate immunity against parasitic infections; however, species-specific differences and complexity of innate immune responses make translation to humans challenging. Thus, there is a need for *in vitro* systems that can elucidate mechanisms of immune control and parasite dissemination. We have developed a human microphysiological system of intestinal tissue to evaluate parasite-immune–specific interactions during infection, which integrates primary intestinal epithelial cells and immune cells to investigate the role of innate immune cells during epithelial infection by the protozoan parasite, *Toxoplasma gondii*, which affects billions of people worldwide. Our data indicate that epithelial infection by parasites stimulates a broad range of effector functions in neutrophils and natural killer cell-mediated cytokine production that play immunomodulatory roles, demonstrating the potential of our system for advancing the study of human-parasite interactions.

## INTRODUCTION

Infections caused by parasitic pathogens are a global health problem that affects more than a quarter of the world's population (1), yet effective antiparasitic therapeutics are limited and often come with severe adverse reactions. Similarly, vaccines are limited for any food or water-borne parasitic infection (1). Immune responses initiated by the innate immune system in the intestinal tissue are a part of the frontline defense against parasitic infections. A more complex picture of their role in shaping protective immunity development and pathogenesis is beginning to emerge. Infection by the protozoan and intracellular parasite *Toxoplasma gondii* affects about a third of humans worldwide, making it one of the most widespread human pathogens in the world (2). Human exposure to *T. gondii* infection occurs primarily through the oral route due to ingestion of contaminated food or water (2). However, there are substantial knowledge gaps in how the innate immune system interacts with human intestinal parasites like *T. gondii* in the local microenvironment of the intestinal tissue that either reduce parasite dissemination or contribute to the development of invasive systemic disease. As responses to parasitic infection by the innate immune system play key roles in shaping protective immunity, improved knowledge of the mechanisms that initiate innate immunity and contribute to pathogenesis is central to developing effective therapeutics and vaccines.

The gut epithelium and vascular barrier regulate what enters the host tissue beyond the intestinal epithelial barrier and what enters the circulation. Functionally, the intestinal epithelial barrier separates the luminal contents from immune cells found in the gut parenchyma and prevents the systemic dissemination of the microbiota and enteric pathogens to the liver, spleen, and other peripheral tissues (3). During parasitic infection, immune cells in the gut parenchyma coordinate host-protective responses necessary for resolving acute infection and preventing tissue dissemination (4). Currently, murine hosts are predominantly used as translational models for *T. gondii* infections in humans. Despite the vast knowledge of basic and translational human immunology obtained from mouse studies, several components of the mouse immune system are incongruent with the human immune system (5, 6). Humanized mice allow for improved modeling of the human immune systems and have emerged as alternatives to traditional rodent models. However, challenges still remain because of the lack of critical adhesion molecules and other signaling proteins in humanized mouse models that are required for mounting human-specific immune responses to infections (7, 8). While *in vivo* animal models replicate microenvironmental complexity and physiological conditions, several aspects including species-specific differences, limited ability to image pathogen trafficking, and the time/expense of mechanistic study make investigation of pathogen trafficking challenging in these models. Thus, there is a need for relevant human *in vitro* models to interrogate the innate immune responses to pathogens.

Organ-on-chip devices and microphysiological systems (MPSs) have overcome some of the challenges of traditional *in vitro* approaches by enabling the integration of three-dimensional (3D) complexity, spatial organization, and relevant cell-cell and cell-extracellular matrix (ECM) interactions for modeling *in vivo*-like responses (9). Several technologies for modeling pathophysiological processes in human tissue have emerged that represent important steps forward in the evolution of organ-on-a-chip platforms. MPS of the lung (10), brain (11), liver (12), and intestine (13) has been developed for studies of host interactions with viruses, fungi, bacteria, and parasites

Copyright © 2022  
The Authors, some  
rights reserved;  
exclusive licensee  
American Association  
for the Advancement  
of Science. No claim to  
original U.S. Government  
Works. Distributed  
under a Creative  
Commons Attribution  
NonCommercial  
License 4.0 (CC BY-NC).

<sup>1</sup>Department of Biomedical Engineering, University of Wisconsin-Madison, Madison, WI, USA. <sup>2</sup>Department of Pathology and Laboratory Medicine, University of Wisconsin-Madison, Madison, WI, USA. <sup>3</sup>Morgan Institute for Research, University of Wisconsin-Madison, Madison, WI, USA. <sup>4</sup>Department of Dermatology, University of Wisconsin-Madison, Madison, WI, USA. <sup>5</sup>Department of Surgery, University of Wisconsin-Madison, Madison, WI, USA. <sup>6</sup>Carbone Cancer Center, University of Wisconsin-Madison, Madison, WI, USA. <sup>7</sup>Department of Medical Microbiology and Immunology, University of Wisconsin-Madison, Madison, WI, USA.

\*Corresponding author. Email: djbeebe@wisc.edu (D.J.B.); ljknoell@wisc.edu (L.J.K.); skerr2@wisc.edu (S.C.K.)

†Present address: Department of Surgery, University of California, San Francisco, San Francisco, CA, USA.

‡Present address: Department of Microbiology and Molecular Genetics, The University of Vermont, Burlington, VT, USA.

(14). In the context of modeling host-microorganism interactions, viral infections and bacterial colonization in the epithelia have been the primary applications of MPSs, with emerging applications in testing antiviral therapeutics and modeling innate immune responses. Immune cell trafficking across endothelial and epithelial barriers has been studied using these models (15), but difficulties persist with integrating membrane-free interfaces that mimic tissue composition of the gut epithelial and vascular barrier, including cellular and ECM components, and tissue architecture (i.e., endothelial vessel and epithelial lumen geometry) that can critically influence host and pathogen responses. Recent efforts to model the 3D tissue anatomy of intestinal epithelia have culminated in the establishment of organoid-on-a-chip systems that retain the cellular diversity and regenerative potential offered by organoid technology while addressing the problem of lumen accessibility using microengineering or tissue engineering approaches (16–18). Using advanced 3D bio-printing techniques, culture of intestinal tubes can be maintained long term in ECM gels within these systems (16). These systems can support in vitro tissue homeostasis of the intestinal epithelium and its interactions with underlying tissue components. However, functional responses of innate immune cells and concomitant molecular analysis of responses to microorganisms in these models have not been characterized.

In this work, we developed an MPS of the human intestinal tissue to study host-parasite interactions and innate immune cell response to parasite infection *in vitro*. By using a highly tractable micromolding technique for creating hollow structures, we generated tubes of intestinal epithelium and endothelium supported by ECM gel, recapitulating the lumen geometries of the gastrointestinal tract and blood vessels. We microengineered a human-relevant model of the gut epithelium and vascular barrier, within the intestinal tissue, that provides means for studying gastrointestinal parasitic infections and the associated interactions with innate immune cells. We demonstrate adaptation of this model to incorporate primary human intestinal stem cells from organoids derived from intestinal tissue resections. We used the system to model parasite invasion and replication within the intestinal epithelium, followed by leukocyte trafficking to the site of infection. Neutrophils and natural killer (NK) cells are critical for early protection and reducing parasite burden during *T. gondii* infection (19, 20). By measuring gene transcription, metabolic changes, and cytokine secretions, we gained interesting insights into the function of human innate immune cells, including neutrophils and NK cells, during the initial stages of *T. gondii* parasite infection of the intestinal epithelium. Hence, the engineered MPS model of the intestinal tissue emulates critical features of host-parasite interactions, enabling us to address questions related to human-relevant tissue response, activation of innate immunity, and the role of immune cells in parasite dissemination.

## RESULTS

### Development of an intestinal tissue MPS for studying host-pathogen interactions

Infection by *T. gondii* is naturally acquired through oral ingestion of food or water that are infected with parasite cysts or oocysts (2, 21). The intestinal epithelium, characterized by a villus-crypt axis consisting of a single layer of constantly renewing and differentiating epithelial cells, separates microbes in the lumen from the intestinal vascular systems (Fig. 1A) (22, 23). Experiments in mice and cell

line/explant studies have shown that translocations of *T. gondii* from the apical surface of the intestinal epithelium to the basal side, during acute infection, may occur via epithelial transmigration or following epithelial invasion and intracellular replication (24). Tissue damage caused by the *T. gondii* epithelial invasion and intracellular replication leads to the secretion of a host of inflammatory factors by intestinal tissue-resident cells (Fig. 1A) (25). The presence of these factors increases the expression of integrins and chemokine receptors on endothelial cells of local vasculature that promote immune cell extravasation into the lamina propria. Leukocytes, primarily neutrophils, are then recruited to the site of infection from neighboring vasculature where they encounter effector-enhancing cytokines and pathogen-derived products to neutralize the parasite by killing or controlling their replication (Fig. 1A) (21, 26). Other innate immune cells such as NK cells are also recruited from the vascular system that further amplifies the inflammatory response by producing effector-enhancing cytokines (Fig. 1A) (27, 28). A robust immune response during these early stages of the *T. gondii* infection is critical for shaping innate immunity, which, in turn, induces acquired immunity.

To model these initial stages of *T. gondii* infection, we bio-engineered an intestinal tissue MPS that incorporates 3D tubular structures of the intestinal epithelium and the endothelium, and immune cell components to allow the analysis of host immune responses against intestinal pathogens in a more physiologically relevant culture microenvironment (Fig. 1B). Inspired by previous work by ourselves and others, we generated lumen structures within a gas- and nutrient-permeable collagen-based ECM hydrogel using a micromolding technique for modeling tubular geometries of the intestinal epithelium and the gut vascular barrier within intestinal tissue (16, 29, 30). The hydrogels are integrated into a polydimethylsiloxane (PDMS) elastomeric device with a central chamber, which contains the ECM gel, connected to two pairs of inlet and outlet ports that support PDMS rods used for molding the tubular structures (Fig. 1Ci). Following ECM gel polymerization, the rods are pulled out of the chamber, leaving behind hollow lumen structures. The inlet and outlet ports connected to the chamber provide direct access to the lumens, which can be used for cell seeding and for the supply of medium and growth factors during culture. We injected and cultured intestinal epithelial cells inside one of the tubular structures to form an epithelial lumen with direct access to the apical surface. After the epithelial lumen is formed, in the same manner, we seeded and cultured vascular endothelial cells in the adjacent lumen to generate a biomimetic endothelial vessel (Fig. 1Cii). To model epithelial invasion of *T. gondii*, we seed parasites into the apical surface of the epithelium through the inlet port and culture them (Fig. 1Ciii). Next, immune cells are introduced directly into the endothelial vessel and cultured for evaluating the immune response (Fig. 1Civ). Together, our model mimics components of the intestinal tissue including the epithelium, adjacent blood vessels, and immune cell components that could provide insight into human innate immune response during infection by protozoan parasites in a more physiologically relevant context.

For initial characterization of the model, we generated tubular intestinal epithelium using the human colon epithelial cell line, Caco-2, and formed a tube-shaped endothelial vessel using human umbilical vein endothelial cells (HUVECs) (Fig. 1D). The ECM hydrogel provides structural support for the formation of continuous layers of epithelial and endothelial cells that functions as a barrier between the apical side of the lumen and the underlying matrix. The intestinal

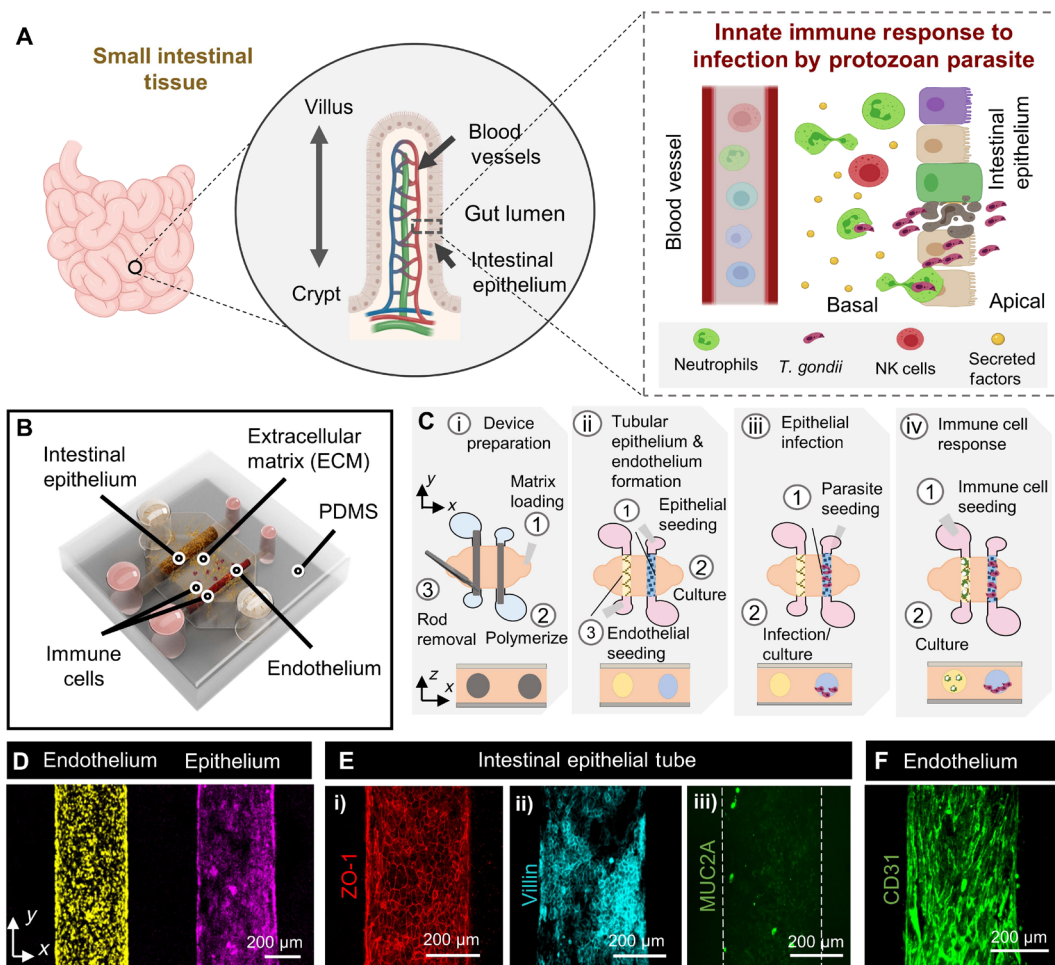


**Fig. 1. Human intestinal tissue MPS for studying innate immune responses to parasitic infection.** (A) Schematic representation of the design rationale for modeling parasite infection, in the intestinal epithelium, and innate immune cell responses. (B) Three-dimensional rendered illustration of the intestinal tissue MPS, within a polydimethylsiloxane (PDMS) device that includes tubular intestinal epithelium and endothelium within an ECM gel. Immune cells are introduced into the lumen of the endothelium for modeling and elucidating innate immune responses to parasite infection of the epithelium. (C) Schematic representation describing the experimental approach to set up each component (i to iv) of the MPS used in this study. (D) Fluorescence image showing the formation of a confluent Caco-2 intestinal epithelium (magenta) and HUVEC endothelium (yellow). (E) The model retains phenotypic characteristics of tight junction markers (i, ZO-1), microvilli markers (ii, villin), and markers of mucus producing goblet cells (iii, MUC2A) for the epithelium. (F) HUVEC endothelium in coculture with the epithelium retains expression of endothelial marker (CD31).

epithelium generated within our system expresses tight junction marker ZO-1, which is involved in barrier function, as well as villin 1 (VIL1) which is involved in microvillus formation and epithelial restitution after damage (Fig. 1E, i and ii). The intestinal epithelium is increasingly recognized as a critical component of mucosal innate immunity against invading microorganisms through the secretion of mucin and antimicrobial proteins. We demonstrate the expression of mucin 2 (MUC2), which is secreted by goblet cells in the intestinal epithelium and forms a major component of the inner mucus layer (Fig. 1Eiii). Expression of these cell lineage markers highlights the characteristic properties of the intestinal epithelium cultured within our system. To assess the characteristic features of the endothelial vasculature, we stained for and observed the expression of endothelial junction protein CD31 (Fig. 1F). Together, these results show that cocultures of tubular intestinal epithelium and endothelium supported by collagen-based ECM gel retain the phenotypic characteristics of a mature epithelium and endothelium.

### Generation and characterization of primary small intestinal tubes in the intestinal tissue model MPS

In vitro cultures of patient or induced pluripotent stem cell-derived intestinal epithelial stem cells in 3D organoids can generate a fully differentiated and polarized epithelium (31–33). However, the relative inaccessibility of the apical surfaces makes the inoculation of larger pathogens, such as *T. gondii* compared to bacteria or viruses, into the cavity difficult to perform. Moreover, the variable 3D geometry of organoids makes real-time imaging of host-pathogen interactions technically challenging. Therefore, we adapted our intestinal tissue MPS to integrate the formation of tubular epithelium using primary human intestinal epithelial cells, from intestinal organoid fragments, to provide a model that retains the major epithelial cell types and provides easy access to the apical surface (Fig. 2A). To incorporate primary human intestinal epithelial cells, we obtained surgical samples from macroscopically normal regions of the human small intestinal tissue. Human intestinal crypts containing functional stem cells,

derived from the jejunum region of the small intestine, were used to generate organoids and cultured for >5 passages before use within our model. Jejunal organoids cultured in an expansion medium for 7 to 9 days were dissociated into a mix of fragments and single-cell suspensions before being introduced into the lumen tube of the microdevice (Fig. 2B). To maximize coverage of the luminal surface, primary small intestinal cells were seeded into the device twice and cultured in expansion media for 24 hours between each cell seeding. The device was flipped upside down before the second round of cell seeding to facilitate cell adhesion to the top half of the lumen surface. Initially, the large majority of cells appear spread across the luminal surface within 1 to 2 days of cell seeding and progressively grow to form a continuous epithelium. Following cell adhesion to

the matrix (approximately 72 hours from initial cell seeding), the culture medium is changed to a differentiation medium (DM), and the intestinal epithelium is cultured for 5 to 7 days to promote differentiation of epithelial subtypes. We used a previously published differentiation culture medium formulation and made further modifications (see Materials and Methods) to accommodate the culture of HUVECs in the adjacent lumen following differentiation of the epithelium. HUVECs were seeded into the adjacent lumen, and the device was inverted every 30 min over a 2-hour period to coat the lumen with endothelial cells. The tubes of intestinal epithelium and endothelium were cocultured for an additional 48 hours before infection with *T. gondii*. For modeling immune response to parasite infection, the intestinal epithelial tube was infected with *T. gondii*

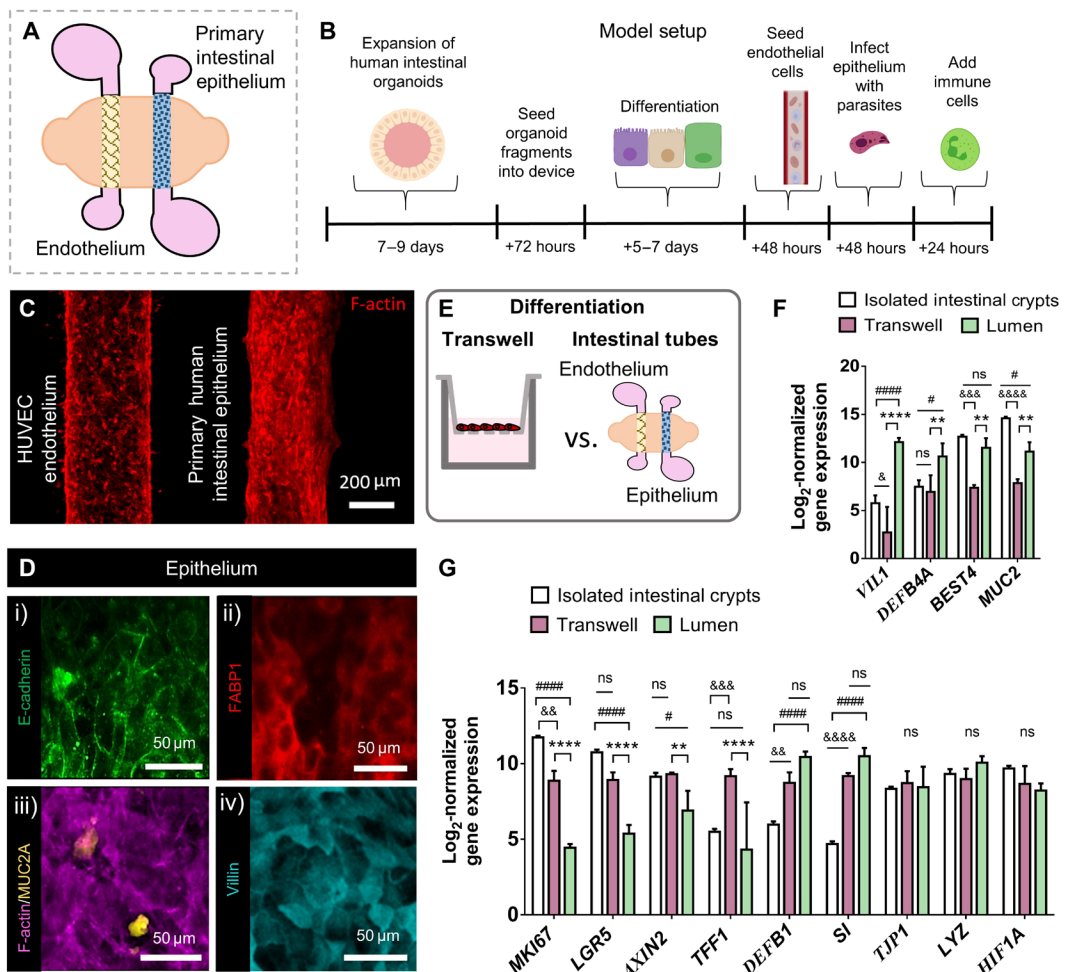


**Fig. 2. Integrating primary intestinal epithelial cells in the human intestinal tissue MPS.** (A) Schematic showing spatial distribution of the intestinal epithelium and endothelium in the intestinal tissue MPS. (B) Optimized culture protocol and timeline to set up the intestinal tissue MPS. (C) Tubular HUVEC endothelium and primary intestinal epithelium cells as shown by immunostaining of F-actin. (D) Differentiated tubular epithelium shows retention of phenotypic characteristics including expression of epithelial cell adhesion protein [i, E-cadherin], enterocyte-specific marker [ii, fatty acid-binding protein 1 (FABP1)], marker for mucin-producing cells [iii, MUC2A], and marker for protein involved in formation of microvilli [villin 1, iv]. (E) Schematic representing the culture and differentiation of human primary intestinal epithelial cells in Transwells and in the intestinal tissue MPS. (F and G) Bar graphs showing differential gene expression in cells isolated from intestinal crypts and in epithelium cultured in the intestinal tissue MPS and Transwells. Genes analyzed include markers associated with the crypt and villus compartment of the intestinal tissue. Values are presented as means ± SD from four independent experiments involving tubular or monolayer epithelium generated from human intestinal organoids (\* = Transwell versus lumen, \*\*\*\*P ≤ 0.0001, \*\*\*P ≤ 0.001, and \*\*P ≤ 0.01; # = isolated crypts versus lumen, #####P ≤ 0.0001 and #P ≤ 0.05; & = isolated crypts versus Transwell, &&&P ≤ 0.0001, &&&&P ≤ 0.001, &&P ≤ 0.01, and &P ≤ 0.05). ns, not significant.

for 48 hours and immune cells including neutrophils and NK cells were added to the lumen of the endothelium followed by coculture within the model for 12 to 24 hours (Fig. 2B).

Cocultures of tubular small intestinal epithelium derived from human primary intestinal epithelial cells with an adjacent vascular lumen can also be established, as shown by immunofluorescent staining of F-actin (Fig. 2C). Immunofluorescence staining confirmed the expression of adherens junction component (E-cadherin) and enterocyte marker (fatty acid-binding protein, FABP1), which are characteristic of intestinal epithelial tissue (Fig. 2D, i and ii). Similar to the Caco-2 epithelial tubes, protein expressions of MUC2 and villin were also observed in epithelial tubes generated from primary intestinal epithelial cells (Fig. 2D, iii and iv).

In vivo, the intestinal epithelium rests on a supporting basement membrane composed of structural and adhesive proteins that epithelial cells use to anchor, migrate, and differentiate (34). Matrix properties such as ECM ligands, stiffness, and porosity are key factors that influence a wide range of cell behaviors including viability, tissue organization/architecture, and stem cell renewal and differentiation (35, 36). The intestinal epithelium is characterized by a villus-crypt axis that is under constant cell renewal, with cells migrating from the proliferative crypt compartment to the functional villus compartment while differentiating. Major cell types of the intestinal epithelium include stem cells, typically enriched in the crypt compartment, to absorptive enterocytes, typically found in the villus compartment, and cells of secretory lineage such as goblet and Paneth cells. To further characterize the change in cell type composition following differentiation in the intestinal tissue MPS, we analyzed gene expression of several established marker genes characteristic of different cell types of the intestinal epithelia including stem cells, goblet cells, Paneth cells, enterocytes, and other markers associated with antimicrobial activity. Details of up-regulated/down-regulated genes and their function in the human intestinal tissue are highlighted in figs. S1 and S2. We compared differentiation of intestinal tubes in our platform and epithelial monolayers in a standard culture platform (Transwell) (Fig. 2E) against stem cell-rich intestinal crypts isolated from small intestinal tissue resections. Small intestinal epithelial cells in the intestinal tissue MPS and the Transwell system were cultured under the same conditions: in the presence of expansion media for 2 days, followed by 7 days of culture in the DM.

Reverse transcription quantitative polymerase chain reaction (RT-qPCR) analysis showed that differentiation in both the tubular (microphysiological model) and the monolayer (Transwell) epithelium generally led to decreased expression of markers for cellular proliferation, *MKI67* (Fig. 2F). In contrast, levels of enterocyte marker, sucrase-isomaltase, and levels of genes that encode for the production of antimicrobial peptides,  $\beta$ -defensin 1 (*DEFB1*), were elevated in the differentiated epithelium in both platforms (Fig. 2G). Moreover, our analysis revealed that, compared to Transwells, differentiation in our model leads to increased gene expression of markers associated with microvilli formation, *VIL1*, and production of antimicrobial peptides, defensin beta 4A (*DEFB4A*) (Fig. 2F). A further decrease in markers associated with stem cell renewal, leucine-rich repeat-containing G protein-coupled receptor 5 (*LGR5*) and crypt regeneration, and axis inhibition protein 2 (*AXIN2*) relative to intestinal crypts was also observed in our model compared to the Transwell condition (Fig. 2G). Levels of absorptive cell marker, bestrophin 4 (*BEST4*), and marker for mucin-producing goblet cells, *MUC2*, decreased significantly in monolayers differentiated in Transwells

but remained at similar levels in our tissue model. Expression of marker for Paneth cells, lysozyme, remained the same in both platforms. Overall, these results suggest that, compared to standard culture techniques, primary intestinal epithelial differentiation in our platform exhibits improved differentiation with attenuated crypt-based stem cell signatures (reflected by decreased levels of *MKI67*, *LGR5*, and *AXIN2* transcripts) and elevated villus-like absorptive/goblet cell signatures (reflected by higher abundance of *VIL1*, *BEST4*, and *MUC2* transcripts).

### Modeling protozoan parasite infection in human intestinal epithelium

Having established that the intestinal tissue MPS recapitulates tubular geometries of the intestinal epithelium and vasculature, the system has strong potential for modeling parasite invasion, replication, and translocation beyond epithelium into the lamina propria (Fig. 3A). *T. gondii* infects the small intestinal epithelium cells following ingestion of parasites found in contaminated meat, produce, or water. During acute infection, *T. gondii* parasites that invade the intestinal epithelium differentiate into a rapidly replicating life stage, referred to as the tachyzoite stage, which then disseminates throughout the body (21, 37). To model *T. gondii* infection of the intestinal epithelium, we introduced tachyzoites into the tubular epithelium of our intestinal tissue MPS. Our model provides an exposed luminal surface accessible to pathogens, allowing us to directly expose the cells to the parasite. Caco-2 epithelial tubes were exposed to approximately  $8 \times 10^7$  transgenic mCherry-tagged *T. gondii* (type II ME49 strain) tachyzoites per tube. The lumen of the epithelial tube was washed with media 12 hours post-infection (hpi) to remove parasites that did not adhere to or invade the epithelium. Discrete and dense areas of parasites could be observed within a small proportion of epithelial cells using fluorescence microscopy at 24 hpi and were largely contained within the boundaries of the epithelial tube (Fig. 3B). The *T. gondii* replicated within the epithelial cells between 24 and 48 hpi. On the basis of the *T. gondii* seeding density used in our study, bright-field images of Caco-2 epithelium do not indicate considerable damage to the epithelium at 48 hpi (fig. S3A). However, as parasite-harboring cells continue to increase, epithelial cell lysis is observed at 72 hpi (Fig. 3C), releasing tachyzoites into the lumen of the epithelium and the basal side of the epithelium. Cell lysis was the primary mode of *T. gondii* translocation across the epithelium observed in our system; however, *T. gondii* transmigration across the epithelium was also observed at times, before cell lysis, when lower *T. gondii* seeding densities were used. To confirm and quantify parasite replication, *T. gondii* genomic DNA in the infected epithelial tubes was quantified at 24 and 48 hpi via qPCR using the *SAG1* (*T. gondii* surface antigen) primer set. qPCR analysis in the infected epithelium showed a sixfold increase in *T. gondii* genomic DNA at 48 hpi relative to 24 hpi (Fig. 3D), confirming our microscopy-based observations. To examine the state of the epithelium, we analyzed the effects of *T. gondii* infection on the barrier function of the epithelium. As a control, uninfected epithelial tubes and epithelial tubes infected with heat-killed *T. gondii* were used (fig. S3, B and C). We measured the permeability characteristic of the epithelial tubes by quantifying transport of fluorescently labeled polysaccharides [fluorescein isothiocyanate (FITC)-dextran, 20 kDa] from the apical side to the basal side of the epithelium (fig. S4). Epithelial barrier function was analyzed at 48 hours for control (uninfected) epithelium and epithelium infected with live *T. gondii* and heat-killed *T. gondii*.

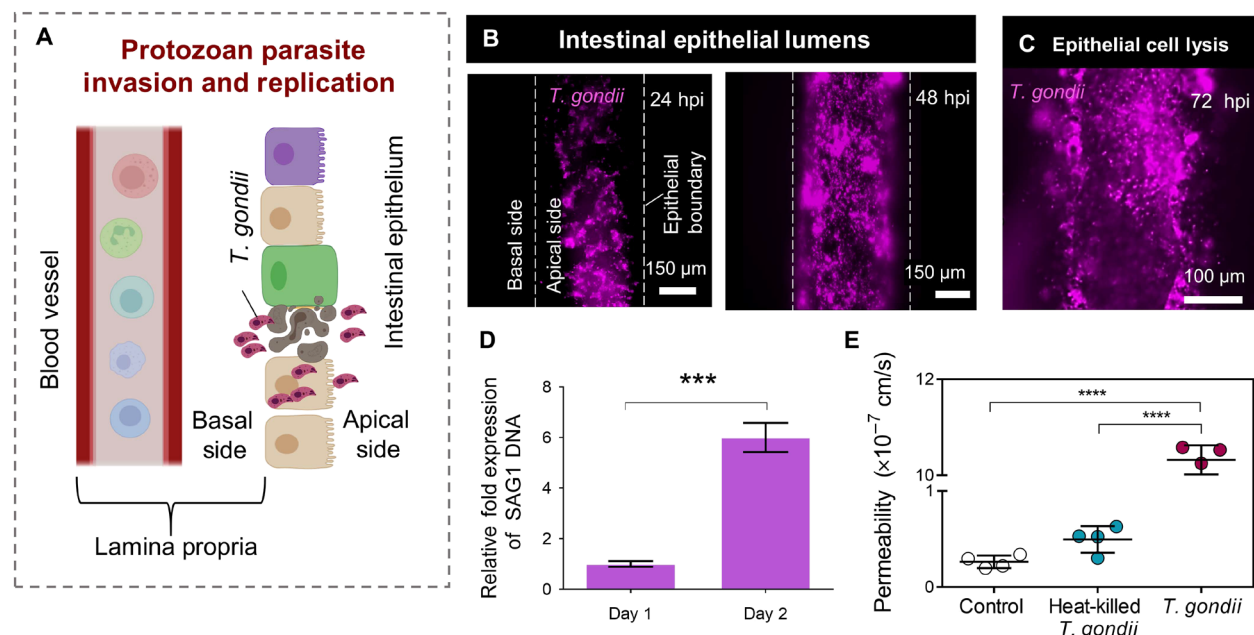


**Fig. 3. Modeling protozoan parasite invasion and replication in the intestinal epithelium.** (A) Schematic representation of epithelial infection by *T. gondii*. Infection involves epithelial invasion, intracellular replication, and transmigration or epithelial cell lysis of *T. gondii*, which releases the parasites into the lamina propria containing immune cells and intestinal vasculature. (B) Caco-2 epithelial tubes were infected with mCherry-tagged *T. gondii* of the ME49 strain for 24 hours and imaged by fluorescence microscopy. The images depict time course images at 24 (i) and 48 hours (ii), showing that viable *T. gondii* was present within the epithelial lumen. White dashed line represents the epithelial boundary separating apical (luminal) surface from the basal surface. (C) Fluorescent image depicting epithelial cell lysis 72 hours following infection with mCherry-tagged *T. gondii*. (D) Relative fold expression of *T. gondii* genomic DNA in the infected epithelial tubes, quantified at 24 and 48 hpi via qPCR using the SAG1 (*T. gondii* surface antigen) primer set. Values are presented as means  $\pm$  SD from two independent experiments and 12 different devices (\*\*P  $\leq$  0.001). (E) Comparison of dextran (20 kDa) permeability through Caco-2 intestinal epithelium under control and infection by heat-killed *T. gondii* or live *T. gondii* conditions. Values are presented as mean permeability  $\pm$  SD (\*\*\*\*P  $\leq$  0.0001).

(fig. S4A). Diffusion of 20-kDa FITC-dextran was tracked over a period of 30 min to analyze epithelial permeability (fig. S4, B and C). Our analysis shows increased permeability in *T. gondii*-infected epithelium compared to uninfected and heat-killed *T. gondii* control conditions (Fig. 3E), suggesting that the infection impairs epithelial barrier function. This also demonstrates our ability to analyze epithelial permeability directly in our platform. Together, these results demonstrate that tubular intestinal epithelium generated in our human intestinal tissue MPS can support the invasion, replication, and translocation of *T. gondii* beyond the epithelium, which are key initial stages of the infection process before the encounter with innate immune cells.

### Neutrophil response to *T. gondii* infection of the intestinal epithelium

Phagocytes involved in innate immunity (i.e., dendritic cells, macrophages, and neutrophils) are the first cells to encounter intracellular pathogens after they cross the epithelial barrier of the intestine. In mice, neutrophils are recruited in abundance to the sites of *T. gondii* infection and account for a high proportion of *T. gondii*-invaded phagocytes in the small intestine following oral entry (Fig. 4Ai) (26). However, little is known about how neutrophils traffic and behave at the gut infection site, and data in mouse studies remain to be validated in human models. Therefore, to gain insight into the behavior and response of human neutrophils to *T. gondii* infection, we used our intestinal tissue MPS to assess neutrophil recruitment behavior to the infection site from a neighboring blood vessel (Fig. 4Aii). We infected Caco-2 intestinal epithelial tubes in our intestinal tissue

MPS with ME49 tachyzoites for 48 hours, as previously described (Fig. 3B). Neutrophils isolated from healthy donor blood were introduced to the endothelial lumen of infected systems and observed for migration behavior over a course of 16 hours. Time-lapse imaging of the intestinal tissue MPS revealed neutrophils migrating within the endothelium and some events of transendothelial migration across the endothelium into the surrounding matrix toward the infected epithelium (Fig. 4B and movies S1 and S2). We observed increased neutrophil speed and displacement from the endothelium in our infected systems compared to uninfected controls (fig. S5). Neutrophil extravasation and migration were also observed in models without epithelium, where a slight, but not significant, increase in migration distance of neutrophils was observed in systems with an epithelium (fig. S6). Migrating neutrophils were seen in the matrix near the infected epithelium, and some small fractions of neutrophils were also observed within the lumen of the infected epithelium (Fig. 4C). Confocal imaging also revealed the presence of fluorescently labeled neutrophils within the infected epithelium colocalized with mCherry-tagged ME49 tachyzoites (Fig. 4C, inset).

When we infected primary small intestinal epithelial cells within the intestinal tissue MPS, a similar increase in end-to-end displacement was observed compared to uninfected systems (Fig. 4, D and E). To directly examine the effects of *T. gondii* infection on gene transcription, we performed RT-qPCR analysis on neutrophils in our model that are responding to infected and uninfected primary small intestinal epithelium. We selected genes that are involved in establishing a protective immunity and activating immune effector functions against invading pathogens. Differential gene expression analysis

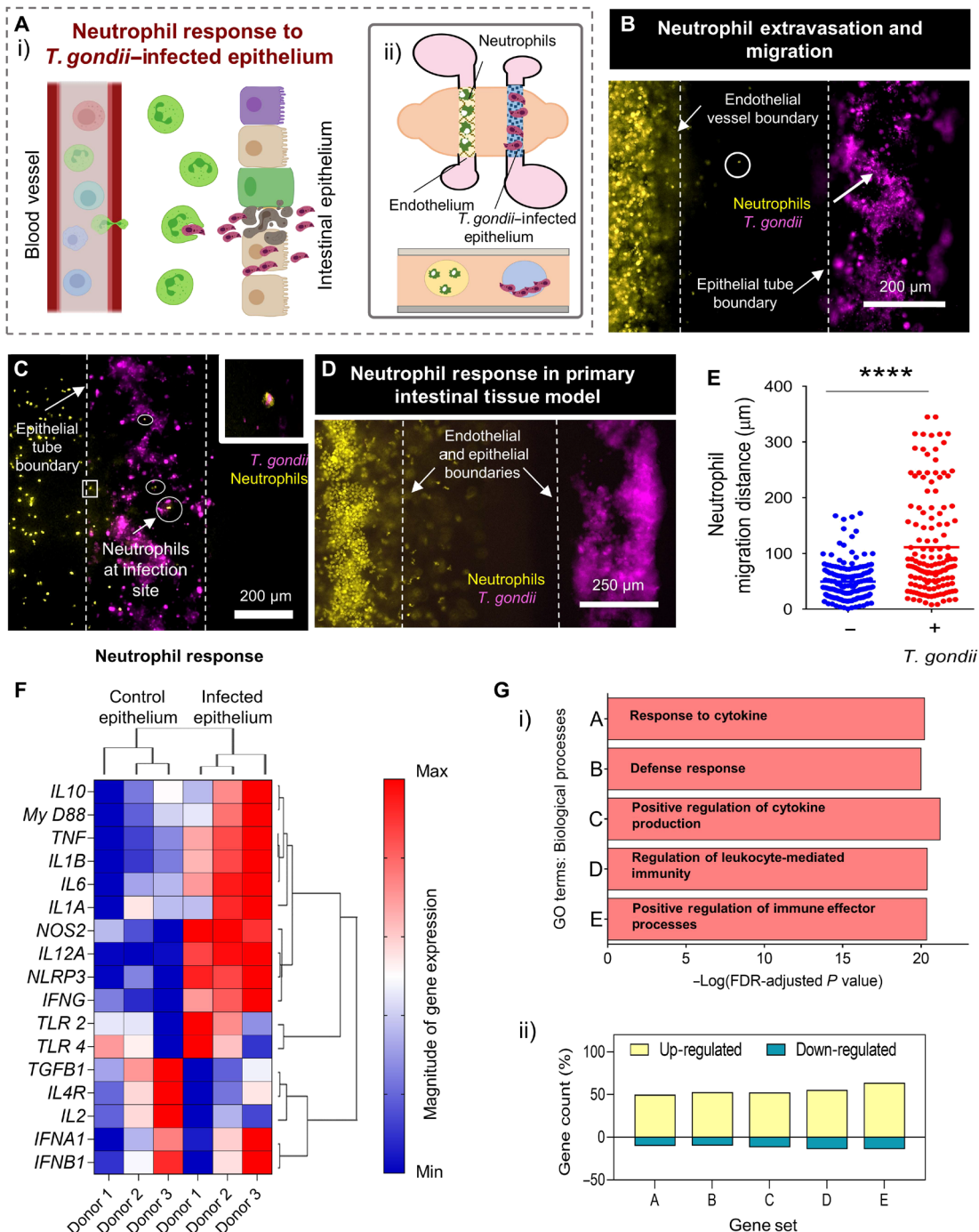


**Fig. 4. Neutrophil response to *T. gondii*-infected epithelium.** (A) Schematic depicting neutrophil trafficking and interaction with a *T. gondii*-infected intestinal epithelium as seen in vivo (i) and as modeled in the intestinal tissue MPS (ii). (B) Confocal image showing extravasated neutrophils and their migration toward a *T. gondii*-infected Caco-2 epithelium. Neutrophils were introduced at 48 hpi and imaged 6 hours after neutrophil seeding. (C) Confocal image showing neutrophils trafficking to the infection site with some neutrophils interacting with the *T. gondii*-infected epithelium. Inset shows colocalization of neutrophils with *T. gondii*. Image was taken 24 hours after neutrophil seeding. (D) Confocal image showing neutrophil extravasation and trafficking toward a *T. gondii*-infected epithelium generated from primary intestinal epithelial cells. Neutrophils were introduced at 72 hpi and imaged 6 hours after neutrophil seeding. (E) Grouped scatter plot showing distance migrated by neutrophils from the endothelium toward *T. gondii*-infected primary intestinal epithelium. Each dot represents the migration distance of a single neutrophil (\*\*\*\* $P \leq 0.0001$ ). (F) Clustergram comparing gene expression in neutrophils from models with *T. gondii*-infected and control epithelium. Neutrophils from three nondiseased donors were used. Gene expression was analyzed for each donor in both control and infected conditions. The dendograms at the top indicate relationship among experimental conditions (control and infected) and, on the left of the figures, indicate relationship among genes (high and low expression). (G) The top five most relevant GO terms associated with the analyzed gene set, and their corresponding  $-\log$  [false discovery rate (FDR)-adjusted  $P$  value] (i). The percentage of genes was associated with each GO term according to their fold changes in expression (increase in yellow and decrease in blue) (ii).

revealed that infection of the intestinal epithelium with *T. gondii* up-regulates multiple genes in neutrophils involved in innate immune responses, including *IL-10* (interleukin-10), *MYD88* (myeloid differentiation primary response 88), *TNF* (tumor necrosis factor), *IL-1B*, *IL-6*, *IL-1A*, *NOS2* (nitric oxide synthase 2), *IL-12A*, *NLRP3* (nucleotide-binding oligomerization domain, leucine rich repeat and pyrin domain containing 3), and *IFN- $\gamma$*  (interferon- $\gamma$ ) (Fig. 4F). Hierarchical clustering analysis revealed distinct gene expression profiles between infected and control conditions. Clustering analysis was conducted using average linkage clustering with Pearson correlation as the default distance metric. We identified the 10 most significant Gene Ontology (GO) terms related to biological processes (table S1A) based on the gene set enrichment analysis molecular signatures database ([www.gsea-msigdb.org/](http://www.gsea-msigdb.org/)). The five most relevant GO terms (Fig. 4G) represent biological processes involving response to cytokines, defense response, positive regulation of cytokine production, regulation of leukocyte-mediated immunity, and positive regulation of immune effector functions (Fig. 4Gi). Most of the genes chosen in our study are involved in these biological processes (table S1B), and the overall gene expression of each of these gene sets was generally up-regulated in neutrophils from the infected models (Fig. 4Gii). These expression patterns suggest that pathways involved in cytokine response, defense response, regulation of leukocyte mediated immunity, and immune effector functions may be active in neutrophils responding to *T. gondii*-infected epithelium. Together, these results show that infection of the intestinal epithelium with *T. gondii* in our intestinal tissue MPS elicits responses consistent with observed in vivo behavior where increased transendothelial migration, trafficking of neutrophils toward the infection site, and activation of pathways involved in defense response to invading pathogens are observed.

### IFN- $\gamma$ -mediated neutrophil response to *T. gondii* infection

In the context of *T. gondii* infection, IFN- $\gamma$  is a cytokine that plays a major role in host resistance and is critical for coordinating protective immunity (38). IFN- $\gamma$  mediates its protective effects by stimulating lysosomal activity (39), inducing expression of nitric oxide synthase and effector genes (40), and modulating metabolic activity (41) in phagocytes. Neutrophils, upon infiltration to the site of infection, execute a broad range of immune effector functions, which include phagocytosis, production of reactive oxygen species or antimicrobial peptides, and activation of programmed cell death pathways to reduce the pathogen's chances of survival (Fig. 5Ai) (42). Here, we investigate the influence of stimulation and inhibition of IFN- $\gamma$  on the effector functions and metabolic activity of neutrophils following an encounter with a *T. gondii*-infected epithelium. To evaluate this, we generated tubular epithelium with Caco-2 cells, infected them with *T. gondii* tachyzoites, as previously described, and introduced primary human neutrophils into the lumen of the epithelium (Fig. 5Aii). As *T. gondii* is an intracellular pathogen, we infected the apical side of the Caco-2 epithelium and allowed incubation for 72 hours, with consistent media replenishment, which resulted in some epithelial cells undergoing cell lysis and exposing *T. gondii* to the luminal contents (Fig. 3C). Neutrophils, isolated from healthy donor blood, were then added into the epithelial lumen to maximize encounter probability with *T. gondii* and cocultured for 6 hours before collection and assessment (Fig. 5Bi). Neutrophil extracellular trap (NET) formation, apoptosis, and parasitization of neutrophils were examined (Fig. 5B, ii to iv, and fig. S7). We first

examined and quantified the fraction of neutrophils undergoing NET formation, which are released from neutrophils in response to invading pathogens. A key step in NET formation is the release of antimicrobial DNA complexes into the cytosol of the cell. Hence, the measurement of decondensed nuclei has been a recognized method for quantifying neutrophils undergoing NET formation (43). We used Hoechst nuclear stain to distinguish between intact and decondensed nuclei, where intact was characterized by normal trilobed nuclei and decondensed was characterized by diffuse staining with large nuclear area (Fig. 5Ci). Neutrophils were stained with Hoechst before introduction into the lumen of *T. gondii*-infected epithelium and removed after 6 hours for analysis. Overall, increased NET formation was observed for conditions with infection. IFN- $\gamma$  stimulation significantly increased the fraction of neutrophils undergoing NET formation compared to control infection. Conversely, blocking IFN- $\gamma$  significantly decreased the fraction of NET-forming neutrophils relative to immunoglobulin G controls and IFN- $\gamma$ -stimulated systems. To evaluate the influence of IFN- $\gamma$  on apoptotic cell death, we examined the induction of apoptosis using a caspase 3/7 activity assay. Our results indicate that blocking IFN- $\gamma$  significantly triggered apoptosis, while IFN- $\gamma$  stimulation suppressed it (Fig. 5Cii). We then examined the effects of IFN- $\gamma$  on the fraction of *T. gondii*-parasitized neutrophils. To eliminate parasites not in contact with neutrophils from analysis, we resuspended neutrophils collected from the epithelium in culture medium and centrifuged them at 200g for 3 min before imaging. Consistent with the trends observed with NET formation, IFN- $\gamma$  stimulation significantly increased the fraction of *T. gondii*-parasitized neutrophils relative to unstimulated systems (Fig. 5Ciii). Blocking IFN- $\gamma$  decreased the fraction of *T. gondii*-parasitized neutrophils compared to IFN-stimulated systems, demonstrating the sensitivity of neutrophils to IFN- $\gamma$  stimulation.

We also investigated the influence of IFN- $\gamma$  on neutrophil metabolic activity by means of optical metabolic imaging, which quantifies relative amounts of reduced form of nicotinamide adenine dinucleotide phosphate [NAD(P)H] and flavin adenine dinucleotide (FAD) (44, 45), and, by extension, the redox ratio. The optical redox ratio is used to obtain information on the dynamic changes in oxidation-reduction rates in cells and is sensitive to alterations in cellular metabolic rates (44). Optical NAD(P)H/FAD redox ratios increased in neutrophils after 6 hours in our IFN- $\gamma$ -stimulated systems indicating increased metabolic activity (Fig. 5D), and these observations were conserved when the analysis was limited to *T. gondii*-internalized neutrophils (fig. S8). Relative to unstimulated systems, lower FAD intensity was observed in response to IFN- $\gamma$  stimulation. Together, these findings suggest that neutrophil effector functions are IFN- $\gamma$  dependent where IFN- $\gamma$  stimulation enhances neutrophil effector functions by increasing events of *T. gondii* internalization, NET formation, and cellular metabolic activity of neutrophils while prolonging their life span. These results demonstrate the utility of our intestinal tissue MPS in testing the sensitivity of immune cells to stimulants that may influence their response to pathogens.

Following an encounter at the infection site, engulfed microbes are carried by migratory phagocytes such as macrophages and neutrophils beyond the epithelia of barrier organs into deeper tissue and draining lymph nodes, contributing to pathogen dissemination to other organs (Fig. 5A) (46). In *T. gondii*-infected mice, parasite-containing neutrophils in the small intestine have been shown to transport the parasite across epithelial barriers to facilitate parasite

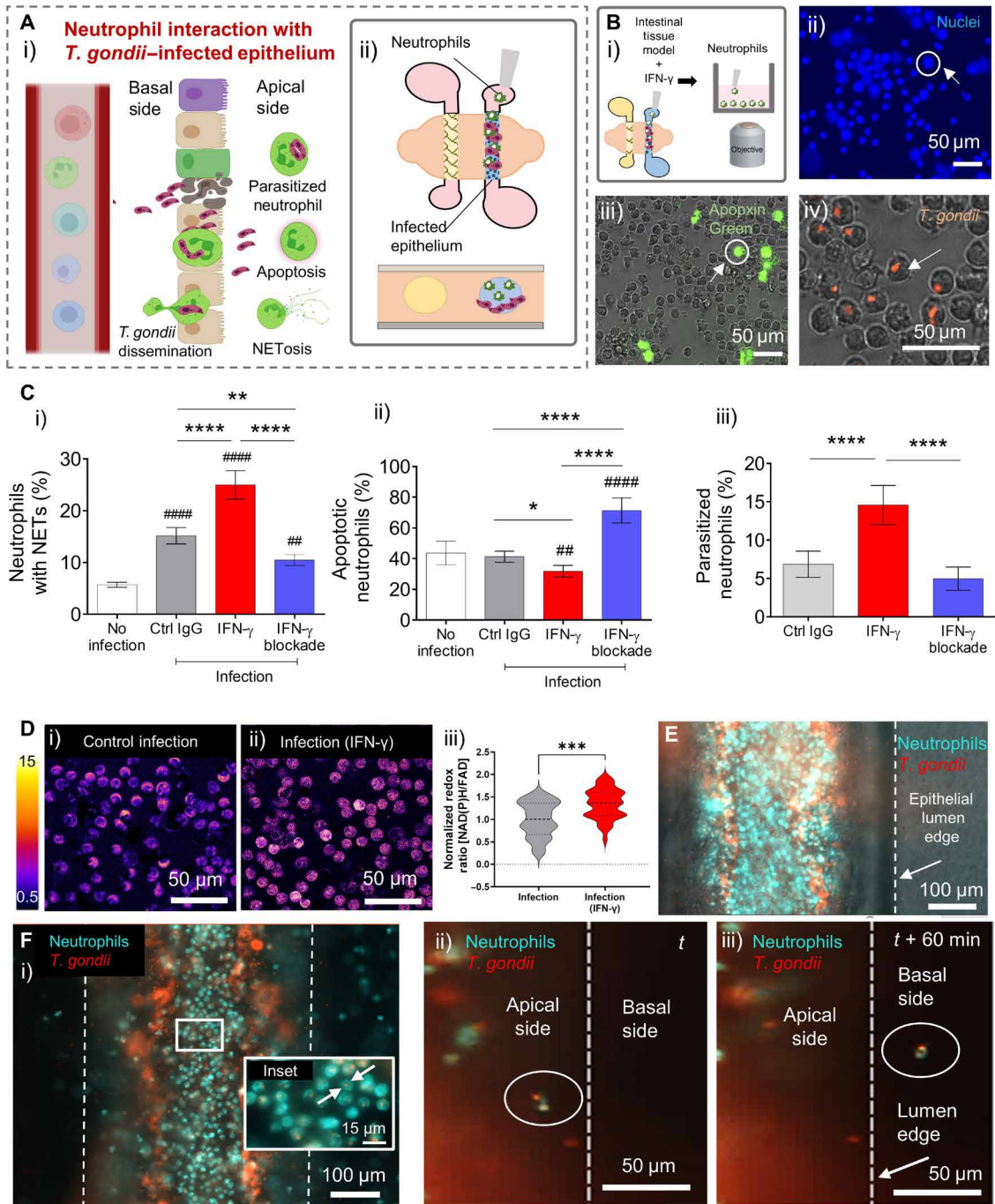


**Fig. 5. Neutrophil effector functions and contribution to *T. gondii* dissemination beyond the intestinal epithelium.** (A) Schematic depicting neutrophil responses at the infection site, as seen in vivo (i), and as modeled in the intestinal tissue MPS (ii). (B) Assessment of neutrophil effector functions (i). Immunofluorescence image showing neutrophil nuclei. White circular line highlights neutrophils with decondensed nuclei (ii). Combined bright-field and fluorescence image showing apoptotic neutrophils. White circle highlights an Apopoxin Green-positive neutrophil (iii). Combined bright-field and fluorescence image showing parasitized neutrophils. White arrow highlights a neutrophil directly interacting with a *T. gondii* parasite (iv). (C) Bar graphs showing percentage of neutrophils undergoing NET formation (i), apoptosis (ii), and parasitization (iii), in response to IFN- $\gamma$  stimulation and blockade. Values are presented as means  $\pm$  SD of neutrophil response from three nondiseased donors (\*\*\*\*P  $\leq$  0.0001, \*\*P  $\leq$  0.01, and \*P  $\leq$  0.05; # = versus no infection control, #####P  $\leq$  0.0001 and ##P  $\leq$  0.01). IgG, immunoglobulin G. (D) Optical metabolic imaging was used to visualize intracellular NAD(P)H and FAD fluorescence intensities of neutrophils in infected systems without (i) and with IFN- $\gamma$  stimulation (ii) [redox ratio = NAD(P)H intensity divided by FAD intensity]. Violin plots showing the analysis of neutrophil redox ratio based on NAD(P)H and FAD intensity (iii) (\*\*P  $\leq$  0.001). (E) Combined bright-field and fluorescence image showing neutrophils within a *T. gondii*-infected epithelium. (F) Fluorescence images showing some neutrophils with internalized *T. gondii* after 6-hour coculture with infected epithelium (i). Fluorescence images showing *T. gondii* trafficking by neutrophils across the epithelial barrier (ii and iii). White dashed line indicates the epithelial boundary separating apical and basal surface (ii and iii).

spread both within the intestine to other regions and beyond to the spleen and mesenteric lymph nodes (26, 46, 47). To investigate whether dissemination of *T. gondii* by migratory neutrophils beyond the epithelium could be observed in our intestinal tissue MPS, we introduced neutrophils into an infected intestinal epithelium generated from Caco-2 cells (Fig. 5E). Within 6 hours, *T. gondii*-containing neutrophils could be seen within the lumen of the intestinal epithelium (Fig. 5F). Time course imaging revealed the translocation of *T. gondii*-containing neutrophils from the apical side to the basal side of the epithelium (Fig. 5F, ii and iii). These results show that our intestinal tissue MPS can recapitulate the mechanisms of parasite dissemination by migratory phagocytes as seen in vivo. Furthermore, our ability to visualize immune cell-mediated transport of pathogens within our intestinal tissue MPS could provide valuable insight into how intracellular pathogens disseminate and present opportunities to investigate previously unidentified targets for therapeutic intervention.

### Innate immune cell response to parasite invasion and replication in the intestinal epithelium

The innate immune system coordinates the first immunological defense against an invading pathogen. As cytokine production by intestinal epithelial and endothelial cells is a key feature of early host immune response, we wanted to evaluate the capacity of our intestinal tissue MPS to produce the inflammatory mediators required for immune effector functions in response to parasite invasion (Fig. 6A). We analyzed inflammatory cytokines secreted in culture media before the addition of immune cells using a Luminex multiplex bead-based enzyme-linked immunosorbent assay. Our results revealed that infection of the primary small intestinal epithelium with *T. gondii* induced significantly higher levels of proinflammatory cytokines/chemokines MCP-1 (monocyte chemoattractant protein-1), MIP-1 $\alpha$  (macrophage inflammatory protein-1 alpha), IL-1 $\alpha$ , IL-1 $\beta$ , GM-CSF (granulocyte-macrophage colony-stimulating factor), IL-6, and IL-8 secretion in culture media at 48 hpi compared to uninfected controls (Fig. 6B). Secretion of anti-inflammatory cytokines such as IL-4, IL-10, and IL-13, on the other hand, showed no change in the infected systems compared to control uninfected systems. Together, these cytokines make up critical components of the inflammatory milieu that contribute to coordinated immune defenses like immune cell trafficking, activation, and effector functions against parasites during acute infection.

Adhesion molecules on endothelial cells are known to mediate leukocyte rolling, adhesion, and subsequent transendothelial migration as part of an inflammatory response to injury or infection. We investigated the effects of infection on the firm adhesion of immune cells to the endothelium. Fluorescently labeled primary human peripheral blood mononuclear cells (PBMCs) were added to the endothelium 48 hpi with ME49 *T. gondii* and washed away after 2 hours to evaluate endothelial adhesion of immune cells (Fig. 6C). The percentage of PBMC adhering to the endothelium doubled relative to systems without infection (Fig. 6D). A similar increase in endothelial adhesion was also observed when NK-92 cells were added to the endothelial vessel (Fig. 6D and fig. S9A). Overall, these results provide strong evidence of epithelial-endothelial cross-talk during parasite infection that promotes immune cell adhesion to endothelium, a critical step in endothelial transmigration and recruitment of immune cells to the infection site. Concurrent with the high levels of proinflammatory cytokines observed in our system, increased levels of soluble adhesion molecules, sP-selectin, sICAM-1, and sE-selectin were also found in the culture media of infected systems (fig. S9B).

Before adaptive immunity is established, NK cells restrain the spread of infection by secreting inflammatory cytokines that are critical for stimulating protective immunity (28). To explore NK cell-mediated production of cytokines in our *T. gondii*-infected intestinal tissue MPS, we compared cytokine secretions in infected systems in the presence and absence of NK cells. NK-92 cells were introduced in the endothelial lumen of infected systems at 48 hpi and cultured for 24 hours (Fig. 6E). Secreted factor analysis was performed on media collected from systems 24 hours after the introduction of NK cells into the lumen of the endothelium. Our results show that the presence of NK cells in infected systems led to significantly higher levels of proinflammatory factors including IFN- $\alpha$ , IL-12p70, TNF- $\alpha$ , IP-10, IL-17A, MIP-1 $\alpha$ , MIP-1 $\beta$ , and IFN- $\gamma$  (Fig. 6F). The presence of NK cells in infected systems also induced significantly higher secretion of IL-10, IL-4, and IL-13, which are known to suppress proinflammatory cytokine production. While the induction of a robust inflammatory response is critical for host resistance against *T. gondii*, unregulated inflammation can result in exacerbated immunopathological reactions causing tissue damage. Thus, anti-inflammatory factors may have critical roles in reducing inflammatory reactions and suppressing collateral damage because of up-regulated inflammation during parasite infection.

### DISCUSSION

Development of improved treatment strategies against parasitic infections requires increased knowledge of the pathogen–tissue-immune system interactions. Murine models have made substantial contributions to our understanding of innate immunity against parasitic infections, but sufficient differences in the organization of the immune system between humans and mice warrant the need for improved models. Therefore, the development of tools that allow researchers to elucidate mechanisms involved in immune responses and defense strategies against parasites and other activators of the immune system in humans could accelerate the development of antiparasitic drugs and therapeutic strategies. In this regard, we have bioengineered an integrated MPS of the intestinal tissue for exploring human innate immune cell responses to parasite infection in the gut. Tubular tissue structures like the intestines and the vasculature system serve essential roles in separation of internal contents and pathogenic microbes in the intestinal lumen from systemic dissemination. Our human intestinal tissue MPS incorporates in vivo-like tubular geometries of the intestinal epithelium and endothelium, allowing us to explore host-parasite interactions and tissue dissemination that occur during the initial stages of infection. Using our model, we examined epithelial infection by *T. gondii*, an intracellular parasite that initially infects the small intestine following ingestion. We introduced a suspension of *T. gondii* tachyzoites directly onto the apical surface of the intestinal tubes, and, using live cell microscopy, we demonstrated that our tubular intestinal epithelium supports invasion and intracellular replication of *T. gondii*. As an important component of the intestinal immune network, the innate immune system is considered the most important defense line against pathogens breaching the epithelial barrier and plays a pivotal role in maintaining immunity and preventing tissue dissemination through the vascular system. Although incorporating tubular intestinal epithelium within scaffolding matrices has previously been reported (16, 30, 48), the originality of our model relies on the integration of vascular and immune cell components. This

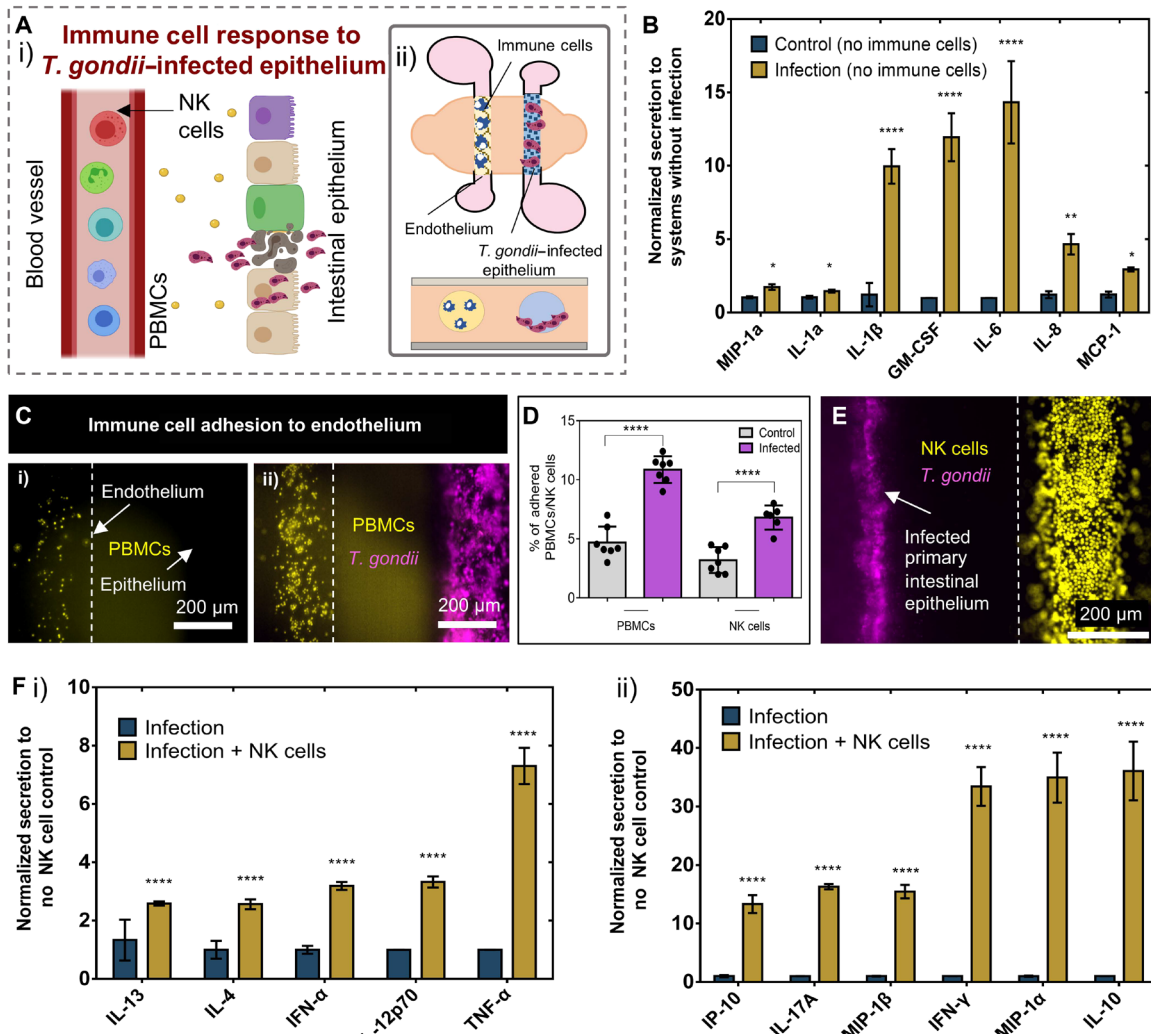


**Fig. 6. Immune cell response and cytokine secretions within the intestinal tissue MPS.** (A) Schematic conceptualization of immune cell response to soluble factor signaling during the initial stages of *T. gondii* infection, as seen *in vivo* (i), and as modeled in the intestinal tissue MPS (ii). (B) Cytokine concentrations measured in media collected from the intestinal tissue MPS consisting of endothelial vessel and primary intestinal epithelial tubes infected with *T. gondii* normalized to control, uninfected systems (\*\*\*\*P ≤ 0.0001, \*\*P ≤ 0.01, and \*P ≤ 0.05). (C) Fluorescence image showing differences in PBMC adhesion events to the endothelial vessel in control (i) and infected (ii) Caco-2 epithelium. (D) Bar graphs showing percentage of PBMCs and NK cells adhering to the endothelium of control and infected systems following coculture for 2 hours. PBMCs and NK cells were added to the lumen of the endothelial vessel after Caco-2 epithelial infection by *T. gondii* for 48 hours. Five devices were prepared on two different days for each condition. \*\*\*P ≤ 0.0001. (E) Fluorescence image showing *T. gondii*-infected primary intestinal epithelial tube in coculture with an endothelial vessel containing NK cells. Epithelial tubes were infected for 72 hours before adding NK cells into the endothelial vessel. (F) Cytokine concentrations measured in media collected from infected intestinal tissue MPS consisting of an endothelial vessel, NK cells, and primary intestinal epithelial tubes infected with *T. gondii* normalized to infected systems without NK cells. In all cytokine measurement experiments, nine devices were prepared on two different days for each paired conditions (infected versus control, and infection in the absence versus presence of NK cells); media from three devices were pooled to make one replicate. Values are presented as means ± SD, \*\*\*\*P ≤ 0.0001.

enables us to investigate the various facets of innate immune cell responses, including extravasation and trafficking, to *T. gondii* infection of the intestinal epithelium and its translocation across the epithelial barrier. One additional design aspect of our system is the compatibility with live cell microscopy enabling dynamic visualization of host-microbe interactions occurring at the interface between the intestinal epithelium and the neighboring vasculature at high spatiotemporal resolution. Using these techniques and molecular analysis, we examined early responses from human innate immune cells like neutrophils and NK cells and investigated parasite-immune cell interactions during epithelial infection that influence immune effector functions and tissue dissemination.

Current in vitro studies of parasitic infections primarily rely on human cell lines that often do not recapitulate *in vivo* phenotypes. On the other hand, maintaining long-term proliferative cultures of the human intestinal epithelium *in vitro* has met with continuing difficulty due to the complex interactions between cell types and the presence of molecular signaling required for stem cell maintenance. Organoid technologies enable the expansion of primary intestinal stem cells and are regarded as a powerful *in vitro* tool for modeling intestinal epithelial tissue due to their structural and functional resemblance to *in vivo* tissue (49, 50). Several studies have used these techniques to study *T. gondii* infection in intestinal organoids (51) as well and in organoid models of the brain and central nervous

systems (52, 53). While apical access can sometimes be limited when using these techniques, methods to form epithelial monolayers from intestinal organoid fragments have been reported (54, 55), where the major epithelial cell types found in 3D organoids are retained when cultured on hard surfaces coated with Matrigel or collagen (56). Building on these methods, here, we adapted our intestinal tissue MPS to integrate the formation of tubular epithelium using primary human intestinal epithelial cells.

We used a simple micromolding-based technique to generate tubular structures within a hybrid matrix, composed of type I collagen, type IV collagen (Col-IV), and Matrigel. Our data indicate this matrix-supported culture and differentiation of human intestinal epithelial cells, both cell lines (e.g., Caco-2) and primary organoid-derived intestinal stem cells obtained from jejunal tissue resections. Maintenance of primary human patient-derived small intestinal cells also requires stimulation from the basal compartment by niche factors that help retain stem cell components while supporting differentiated enterocyte-goblet cell function (32, 49). To support the integration of the endothelial vessel and immune cells (i.e., neutrophils, NK cells, and PBMCs) into our systems, we optimized culture protocols and media compositions for differentiating a primary intestinal epithelium and to support all cell types within the intestinal tissue MPS. Although several molecular and functional properties of the intestinal epithelium within the system are expected to change because of constantly evolving differentiation states and influence from coculture with other cell types, we confirmed through visual inspection of the system that the epithelium and endothelium remain intact. Furthermore, we show that phenotypic characteristics and barrier properties of both the epithelium and endothelium are retained for the duration of the experiments (5 days after endothelial cell seeding), which correlates with the turnover of intestinal epithelia *in vivo* (57). Intestinal tubes generated within the hybrid matrix, both from the Caco-2 cell line and primary intestinal stem cells, exhibited key properties of the intestinal epithelium including a polarized epithelium expressing markers of tight junctions, goblet cells, and microvillus formation. Gene expression analysis showed that expansion of primary intestinal stem cells in tubular structures resulted in improved differentiation of the epithelium, with elevated villus-like absorptive/goblet cell signatures and attenuated crypt-based stem cell signatures, compared to monolayers formed in Transwells. These results agree with previous reports showing that a suitable matrix with relevant ECM proteins and biophysical properties are key factors in providing physical support and facilitating the differentiation of intestinal stem cells (36).

By integrating blood vessels, circulating innate immune cells, and primary intestinal epithelial cells within a biomimetic 3D scaffolding matrix, we incorporated key cellular components and relevant cell-ECM interactions of the intestinal tissue for improved modeling of host-parasite interactions and innate immune cell responses. We also demonstrated impaired epithelial barrier function caused by *T. gondii* infection. Initial responses against *T. gondii* are managed by innate immune cells, with neutrophils, dendritic cells, and monocytes playing a central role (6, 58). Early depletion studies in mice using monoclonal antibodies showed that neutrophils are important for host survival during acute infection (59). Further highlighting their importance, depletion of neutrophils showed decreased levels of IFN- $\gamma$ , IL-12, and TNF, indicative of a weaker type I immune response, and development of lesions in multiple organs including the lung, liver, and brain. Using our intestinal tissue MPS, we recapitulated events

with human neutrophils including extravasation and migration toward the *T. gondii*-infected epithelium, reminiscent of the process of leukocyte trafficking to the site of infection previously observed in mouse models (26). To reduce donor-to-donor variability from adult intestinal stem cells, we used organoid-derived stem cells from a single donor to generate tubular intestinal epithelium, but neutrophils from multiple blood donors were used to ensure consistency in donor-to-donor response to infected epithelium. Our results show that infection of the primary small intestinal epithelium by *T. gondii* up-regulates the expression of several genes in neutrophils that are involved in cellular processes including positive regulation of cytokine production, response to cytokines, regulation of leukocyte mediated immunity, defense response, and positive regulation of immune effector functions.

Although our pathway enrichment analysis was conducted on the basis of a small gene set, future studies could further explore these processes using Kyoto Encyclopedia of Genes and Genomes pathway analysis. Recent *ex vivo* work exploring immune evasion strategies of *T. gondii* suggests that the parasite may prolong the life span of neutrophils by delaying apoptosis in infected cells (60). The study examined transcriptional responses of *T. gondii*-infected human neutrophils and showed up-regulation of pathways involved in mediating immune responses and cellular response to stress that are consistent with some of the pathways implicated in our analysis. However, down-regulation of pathways associated with myeloid leukocyte activation, cytokine secretion, and activation of apoptotic caspases was also observed in neutrophils after they have been actively infected by *T. gondii*. As our study primarily examined the responses of neutrophils to *T. gondii*-infected tissue, future studies exploring responses of *T. gondii*-infected neutrophils in our platform would provide insight into the mechanisms of human innate immune evasion strategies used by *T. gondii*.

Our study also highlighted changes in the functional behavior of neutrophils that correlate with the biological process involved as determined by gene expression analysis. In line with the transcriptional changes observed, dynamic visualization of neutrophil behavior at the epithelial and vascular interface showed increased migration speed and end-to-end displacement from the endothelium in response to the infection of the epithelium. Notably, some instances of direct interaction between neutrophils and excysted *T. gondii* within and near the epithelium could also be observed, demonstrating the capability of our model in capturing parasite invasion, replication, and initial response of neutrophils in the same experiment.

Host-directed therapies that target signaling pathways for parasite clearance bypass many problems encountered by antiparasitic drugs including poor patient compliance and the emergence of drug-resistance parasites (61). By targeting host pathways that are redundant in the host but are critical for parasite survival, there is a reduced chance of developing treatment resistance due to the slow rates of mutations in molecules and processes in the host relative to parasites. In this work, we examined the effects of a host-targeted pathway on the effector functions of neutrophils. Once at the site of infection, local production of inflammatory mediators regulates intercellular communication that mobilizes several defense mechanisms in tissue-resident cells and immune cells. IFN- $\gamma$  has a multitude of immunomodulatory functions and is considered one of the most potent pleiotropic cytokines (38, 62, 63). IFN- $\gamma$  interactions with T cells, NK cells, and activated macrophages have been widely researched; however, investigations into the role of IFN- $\gamma$  during the initial

responses of neutrophils and other innate immune cells to infection by parasites have been limited. We demonstrated the influence of IFN- $\gamma$  on traditional neutrophil functions including parasitization, NET formation, and apoptosis of neutrophils. IFN- $\gamma$  treatment favorably affected neutrophil functions with increased parasitization, NET formation, and overall metabolic activity in neutrophils. In contrast, neutrophil apoptosis, the process of programmed cell death, decreased, which limits exposure of destructive neutrophil productions to surrounding tissue. IFN- $\gamma$  blockage reversed these trends, further highlighting the importance of IFN- $\gamma$  on traditional neutrophil functions of antimicrobial activities and showing the utility of our model for investigation of human immune responses. We also demonstrate the ability of our model to investigate parasite dissemination facilitated by neutrophils, both within the lumen of the intestinal epithelium and beyond by crossing the epithelial wall into the surrounding tissue. These observations are also consistent with data in mice that show the involvement of neutrophils in the spread of *T. gondii* infection with the intestinal tissue (26). Together, we demonstrate the sensitivity of our system in capturing the changes in various effector functions and antimicrobial activity of neutrophils in response to inflammatory stimulus and blockage.

Our secreted factor analysis revealed that our intestinal tissue MPS produces a wide array of proinflammatory cytokines/chemokines (MCP-1, MIP-1 $\alpha$ , IL-1 $\alpha$ , IL-1 $\beta$ , GM-CSF, IL-6, and IL-8) that enhance and activate defense mechanisms in innate immune cells during *T. gondii* infection. In mice, these factors are known to have immunoregulatory roles during acute infection. For instance, the production of MCP-1 and MIP-1 $\alpha$  in our system is consistent with in vivo data in mice showing higher expression of these chemokines in *T. gondii*-infected intestinal epithelial cells (64). Also, mice deficient in MCP-1 and its chemokine receptor CCR2 fail to generate adequate immune response during acute *T. gondii* infection (65), highlighting its critical role in regulating innate immunity. Elevated levels of IL-1 $\alpha$  and IL-1 $\beta$  have been previously observed in the serum of *T. gondii*-infected mice (1 week after infection) and are known inflammatory mediators/regulators of host tissue homeostasis during acute infection (66, 67). Moreover, chemokines like GM-CSF, IL-6, and IL-8, aside from their involvement in inflammation, play important roles in the recruitment and enhanced survival of phagocytic cells like neutrophils during acute innate response to *T. gondii* infection (68–70). Together, these cytokines make up critical components of the inflammatory milieu that contribute to coordinated immune defenses like immune cell trafficking, activation, and effector functions against parasites during acute infection. In accordance with the increased levels of these cytokines in our infected systems, we observed increased neutrophil trafficking and transcriptional changes associated with responses to cytokines and positive regulation of immune effector functions in neutrophils. While we have not explored the direct influence of these cytokines on the functional behavior of neutrophils, future studies using our model could explore spatial and temporal relationships between neutrophils and infection-derived factors that enhance their overall effector functions against parasites.

During innate immune responses, *T. gondii* infection-induced production of inflammatory cytokines drives NK cells to produce a host of factors such as IFN- $\gamma$  and TNF- $\alpha$  that amplify effector functions and inflammatory responses driven by other innate immune cells. NK cell production of immunosuppressive cytokines that counterbalance inflammatory responses during disseminated pathogenic infection with *T. gondii* has also been found (71), shedding light on

the role of NK cells in facilitating immunoregulation. While the mechanisms have not been clearly defined, the immunoregulatory roles of NK cells are likely important for preventing inflammation-dependent pathology during parasite infection. Further exploration of secreted factor analysis shows that incorporating NK cells into our systems up-regulates several immunoregulatory signaling factors critical for amplifying the production of inflammatory and enhancing effector functions in other innate immune cells. In the presence of NK cells, several cytokines (IFN- $\alpha$ , TNF- $\alpha$ , IFN- $\gamma$ , IL-17A, IP-10, IL-4, IL-13, IL-12p70, and IL-10) were uniquely elevated in our infected systems. IFN- $\alpha$ , a member of the type I IFN family, has recently been shown to enhanced cytokine secretion and cytotoxic potential in NK cells (72), and TNF- $\alpha$  together with IFN- $\gamma$  are major proinflammatory cytokines produced by NK cells as means of host protection against *T. gondii* (28). Moreover, these two cytokines are recognized as essential immune effectors against intracellular pathogens. IL-17 has been implicated in resistance to *T. gondii* where IL-17R $^{-/-}$  mice showed defects in neutrophil recruitment and increased parasite burden (73). As NK cells are often considered to function at the interface of the innate and adaptive immune response, NK cell production of chemokine, IP-10, can be critical for generating an adaptive immune response and influencing the recruitment of effector T cells to the *T. gondii* infection site (74). Cytokines typically involved in the resolution of cell-mediated inflammation [IL-4, IL-13, and IL-10 (75)] were also elevated in our infected systems with NK cells. Conventionally, IL-4 and IL-13 are thought to counter NK cell effector functions by limiting the production of IL-12. However, recent work shows that stimulation with IL-4 or IL-13 enhances TNF- $\alpha$  and IFN- $\gamma$  production in NK cells in the presence of IL-12, underscoring the immunoregulatory roles of these cytokines (76). Elevated IL-10 levels observed are also in line with previous reports showing that NK cells produce IL-10 during acute *T. gondii* infection, which interferes with the activation of the adaptive immune responses (77), further highlighting the immunoregulatory roles of NK cells. While the source of these cytokines is unclear in our analysis, secretion of these factors is markedly higher in our infected intestinal tissue MPS with NK cells, indicating a direct or indirect contribution from NK cells. The local effects of this inflammatory environment on the effector functions of neutrophils and other innate immune cells may be tested with future experiments within our platform and using tools/methods for examining complex interactions in vitro.

Collectively, our secreted factor analysis demonstrated a wide array of immunoregulatory cytokines, chemokines, and adhesion molecules generated within our primary intestinal tissue MPS during *T. gondii* infection, which are essential for generating a robust immune response. These molecules are critically involved in innate immunity against intracellular pathogens in the following ways: (i) promoting leukocyte adhesion to the endothelium and transendothelial migration; (ii) trafficking, recruitment, and survival of phagocytic cells; and (iii) enhanced activation, cytotoxic activity, and effector functions of immune cells involved in the innate and adaptive immune responses. These data confirm the presence of an immunomodulatory cytokine milieu that can support mounting a strong immune response to parasitic infections.

However, this study has several limitations. First, while we have examined some aspects of neutrophil and NK cell responses in our model, other biological factors such as the microbiome, tissue oxygen levels, and other immune cell components (i.e., monocytes, macrophages, and dendritic cells) could influence mechanisms of parasite

interaction with the epithelium and innate immune cell responses observed in our models. In future studies, these components may be integrated in our model to better recapitulate the *in vivo* microenvironment and to examine their influence on parasite immunity. Another limitation of our study is that our transcriptomic and cytokine profiling analysis examined a limited number of genes and factors that only represents a fraction of the total number of alterations involved in establishing protective immunity and generating a robust immune response. RNA sequencing analysis and examination of additional immunomodulatory factors can help provide a more in-depth molecular analysis of the biological processes activated in neutrophils and NK cells during *T. gondii* infection in our model. Last, human *in vivo* data on innate immune responses to *T. gondii* infection, in particular during the early stages of the infection that we are modeling, remains limited, making it challenging to compare our observations against *in vivo* data. The neutrophil and NK cell responses observed in our model will need to be validated using humanized mouse models or clinical studies.

The primary objectives of this work were to create an MPS that recapitulates complex interactions between key components of the human intestinal tissue and to demonstrate its usefulness in studying innate immune responses to parasitic infection. Recreating the initial stages of parasitic infection by *T. gondii* and the accompanying innate immune responses of the intestinal tissue highlights the potential of our microphysiological model to fill the gaps in studying human tissue responses through mechanistic correlations between various molecular and functional cell data to both animal and human clinical data. Our readily accessible approach to generating 3D geometries of tubular organs within biomimetic ECM scaffolds could answer questions that have so far been difficult to address. Combined with the ability to dynamically visualize and explore immune responses to host-microbe interactions at a high spatiotemporal resolution, our model may have substantial potential for discovery of cell-mediated immune responses and development of host-directed therapies.

## MATERIALS AND METHODS

### Intestinal tissue MPS fabrication and assembly

The intestinal tissue MPS was fabricated using a micromolding technique to generate tubular structures with an ECM scaffold. This approach enables fabrication of one or more lumen structures with variable size, configuration, and lumen spacing controlled by micro-mold design in soft lithography. Here, we use a two-lumen setup, each lumen equipped with a separate inlet and outlet port, within a single chamber with perpendicularly oriented side ports. Two stacked PDMS layers, with microscale features patterned into them, formed the culture chambers in which scaffolding ECM gel can be loaded, while removable PDMS rods formed the hollow lumen structures surrounded by the ECM gel. The master molds for the PDMS layers were made using SU-8 100 (Microchem), which were spin-coated onto wafers, soft-baked (i.e., heat at 65°C for 30 to 40 min and then at 95°C for 90 to 120 min depending on layer thickness), exposed to ultraviolet (UV) through a mask of desired patterns, and post-baked at 95°C for 20 to 30 min. This procedure was repeated for additional layers before development in propylene glycol monomethyl ether acetate (MilliporeSigma). After developing, PDMS (Sylgard 184 Silicon Elastomer Kit, Dow Corning Corporation) was applied to the masters at a ratio of 10:1 base to curing agent and allowed to polymerize for 4 hours at 80°C. The rods were drawn from needles with gauge size,

23G (340-μm inner diameter). Before device assembly, the PDMS layers and rods were soaked in 100% ethanol for several days to extract any uncured PDMS oligomers. Following PDMS extraction, the rods were placed in between two layers, across the body of the chamber (3 mm in length) in ledge features stemming from the smaller inlet and larger outlet ports to hold the rods in the middle of the chamber. The side ports (4 mm apart) of the chamber were used to fill the chamber with ECM gel, and the height of the chamber was about 1.25 mm. Once assembled, the PDMS layers were oxygen-plasma-bonded onto a glass-bottom MatTek dish using a Diener Electronic Femto Plasma Surface System.

### ECM gel preparation and loading

The bonded devices were UV-sterilized for 20 min and moved to the biosafety cabinet before ECM gel loading. To promote matrix adhesion to PDMS, the device chambers were treated with 1% polyethylenimine (MilliporeSigma) in deionized (DI) water solution for 10 min, followed by a 30-min treatment of 0.1% glutaraldehyde (MilliporeSigma) in DI water solution. Following surface treatment, devices were flushed with DI water solution five times to remove excess glutaraldehyde. A high concentration rat tail collagen I (Col-I) (Corning) neutralized with 0.5 N sodium hydroxide (Thermo Fisher Scientific) was mixed with 7.5 pH 5× phosphate-buffered saline (PBS), complete growth medium or organoid expansion medium, human placental Col-IV, and Matrigel to achieve a final ECM solution containing Col-I (4 mg/ml), 15% Matrigel, and Col-IV (50 μg/ml). The pH of the ECM mix was adjusted to pH 7.2 before loading the mix into the gel chamber of the device. The devices were first kept at room temperature for 20 min and then moved to an incubator at 37°C for at least 1 hour before cell loading. To prevent dehydration during polymerization, PBS was added to the MatTek dish surrounding the devices. PDMS rods were then removed, leaving behind hollow tubular structures within the ECM gel that can be lined with cells.

### Crypt isolation and gut organoid culture

Small intestinal crypts were isolated using a previously established protocol (78) from jejunal tissue resection samples removed from nondiseased tissue of deidentified individuals. Jejunal tissue resections were performed at University of Wisconsin-Madison upon the donors' informed consent, and methods were carried out in accordance with Institutional Review Board (IRB) (protocol no. 2016-0934). Small intestinal organoids were established from isolated crypts by resuspending in Matrigel (Corning; growth factor-reduced, phenol red-free formulation) and culturing in 24-well plates (Polystyrene, Nunc, nontreated multidishes, Thermo Fisher Scientific) at 37°C in the organoid expansion media. Expansion medium consisted of a mixture of base medium [BM; 45% (v/v)], L-WRN conditioned medium [CM; 45% (v/v)], supplement mix, 1× Primocin (InvivoGen), and 10% heat-inactivated fetal bovine serum (FBS; MilliporeSigma). BM was prepared from Advanced Dulbecco's modified Eagle's medium (DMEM)/F12 (Thermo Fisher Scientific) supplemented with GlutaMAX (2 mM; Thermo Fisher Scientific), Hepes (10 mM; Thermo Fisher Scientific), penicillin/streptomycin (Pen/Strep) (Thermo Fisher Scientific), B-27 Supplement (Thermo Fisher Scientific), N-2 supplement (Thermo Fisher Scientific), and 1% cell-culture grade bovine serum albumin (BSA). L-WRN CM was prepared using L-WRN cells from American Type Culture Collection (ATCC; catalog no. CRL-3276) and a previously published protocol (79). The supplement mix consisted of epidermal growth

factor (50 ng ml<sup>-1</sup>; PeproTech), N-2 supplement (Thermo Fisher Scientific), human [ $\text{Leu}^{15}$ ]-gastrin I (10 nM; MilliporeSigma), *N*-acetyl cysteine (500  $\mu\text{M}$ ; MilliporeSigma), nicotinamide (10 mM; Thermo Fisher Scientific), A 83-01 (500 nM; Tocris), SB202190 (10  $\mu\text{M}$ ; Selleckchem), prostaglandin E2 (10 nM; Tocris), Y-27632 (10  $\mu\text{M}$ ; Selleckchem), and CHIR99021 (5  $\mu\text{M}$ ; Tocris). Jejunal organoids were split every 7 to 9 days as previously described (31). On the basis of this established protocol, Matrigel plugs containing organoids were digested in 0.5  $\mu\text{M}$  EDTA (Invitrogen) and collected. After centrifugation at room temperature for 3 min at 300g, supernatant was removed followed by incubation in trypsin (Sigma-Aldrich) for 2 min at 37°C. Trypsin was neutralized using Advanced DMEM/F12 supplemented with 20% FBS and 1% Pen/Strep followed by mechanical dissociation of organoids by vigorous pipetting (about 30 times) to make small organoid fragments. After centrifugation at room temperature for 3 min at 300g, pellets were reconstituted in 50:50 mix of fresh Matrigel and expansion medium at 1:3 to 1:4 ratio and cast in 25- $\mu\text{l}$  droplets in a 24-well plate. Matrigel droplets containing organoid fragments were then polymerized for 15 min at 37°C before adding 500  $\mu\text{l}$  of expansion media to each well. Expansion media were changed every 2 to 3 days, and organoids were used between passages 5 and 25. Y-27632 was only used for the first 48 hours after single-cell dissociation to prevent detachment-induced cell apoptosis.

### Caco-2 epithelial tube formation

Caco-2 cell line was acquired from the ATCC and maintained in Eagle's minimum essential medium (EMEM; MilliporeSigma) supplemented with 20% FBS and 1% Pen/Strep. To generate tubular epithelium, Caco-2 cells were detached using a trypsin/EDTA solution and resuspended at 17 million cells/ml of supplemented EMEM. After removal of the PDMS rod, 3  $\mu\text{l}$  of cell suspension was introduced into the hollow tubes through the inlet ports, and cells were allowed to fill the lumen structures by passive pumping. The microdevice was rotated every 30 min over a 2-hour period to line the hollow tube with epithelial cells. Nonadherent cells were washed off with culture medium, and excess medium was added to the inlet/outlet ports. After completion of tube formation (~24 to 48 hours), the epithelial tubes were cultured in supplemented EMEM with reduced FBS to 10% for 5 to 7 days before coculture with endothelial vessels.

### Primary intestinal epithelial tube formation

Jejunal organoids were collected at days 7 to 9 after passaging and dissociated into small organoid fragments as described above. Pellets of organoid fragments were resuspended in expansion medium at a density of 5 million cells/ml. As previously described, 3  $\mu\text{l}$  of organoid cell suspension was introduced into the hollow tubes through the inlet ports. Cells were allowed to settle on the bottom half of the tubular structure for 24 hours at 37°C in 5% CO<sub>2</sub> after expansion medium was added to the gel ports and the inlet/outlet ports during culture. After 24 hours, nonadherent cells were gently washed with expansion medium. Fresh organoid fragments were prepared and seeded again into the tube. Expansion medium was added to the ports and the microdevice cultured for an additional 24 hours while flipped upside down to facilitate adhesion of cells to the top half of the hollow tubular structure. After completion of tube formation (~72 hours), the primary intestinal epithelium was cultured in DM for 5 to 7 days. For differentiation, the culture medium was replaced with BM [80% (v/v)], L-WRN CM [10% (v/v)], supplement mix (without Y-27632 and reduced CHIR 99021 to 500 nM), 1× Primocin (InvivoGen), and 10%

heat-inactivated FBS (MilliporeSigma). DM was changed twice daily. After 5 to 7 days of differentiation, HUVECs (Lonza) were added to the adjacent hollow tube to generate cocultures of epithelial and endothelial tubes.

### Coculture of epithelial tubes with endothelial tubes

HUVECs were maintained in EGM-2 MV BulletKit medium (Lonza) and used until passage 8. To generate coculture of primary intestinal tubes with endothelial vessels, HUVECs were detached using a trypsin/EDTA solution and resuspended at 15 million cells/ml of modified DM. Modified DM was made by replacing BM in the DM formulation with EGM-2 MV BulletKit medium. Three microliters of endothelial cell suspension was introduced into the cell-free hollow tube next to the epithelial tube, and device was rotated every 15 min over a 2-hour period as previously described. Modified DM was added to the gel ports and epithelial inlet/outlet ports during this process to nourish the epithelial cells. After lining the tube with endothelial cells, nonadherent cells were gently washed with modified DM. The epithelial and endothelial tube cocultures were maintained in modified DM for the remainder of the experiments unless otherwise stated. To support coculture of HUVEC vessels with Caco-2 epithelial tubes, the supplemented EMEM with reduced FBS was mixed with EGM-2 MV at 50:50% (v/v) dilution and used as culture medium for the remainder of the experiments.

### Coculture of epithelial and endothelial tubes with NK cells

NK-92 cell line was acquired from the ATCC and maintained in X-VIVO 10 (Lonza) supplemented with 20% FBS and 0.02 mM folic acid (MilliporeSigma) dissolved in 1 N NaOH, 0.2 mM myo-inositol (MilliporeSigma), and IL-2 (100 U/ml; PeproTech). NK cells were collected and after centrifugation at room temperature for 3 min at 300g, pellets were resuspended in modified DM supplemented with 0.02 mM folic acid, 0.2 mM myo-inositol, and IL-2 (100 U/ml). Resuspended cells were introduced into the endothelial vessel and coculture for 24 hours in excess medium.

### Neutrophil isolation

All blood samples were drawn according to IRB-approved protocols per the Declaration of Helsinki at University of Wisconsin-Madison. Neutrophils were purified from whole blood using the MACSxpress Neutrophil Isolation Kit per the manufacturer's instructions (Miltenyi Biotec), and residual red blood cells were lysed using the MACSxpress Erythrocyte Depletion Kit (Miltenyi Biotec). Blood was drawn from a total of three nondiseased donors with informed consent obtained at the time of the blood draw according to requirements of the IRB. Before loading, the purified neutrophils were stained with calcein acetoxymethyl ester at 10 nM (Thermo Fisher Scientific) according to the manufacturer's instructions. Neutrophils were resuspended in 50:50% (v/v) EMEM and EGM-2MV culture medium for coculture with Caco-2 epithelium or resuspended in modified DM for coculture with primary intestinal epithelium.

### Parasite cell culture and infection

*T. gondii* ME49 tachyzoites were propagated in human foreskin fibroblast monolayers grown in DMEM containing 10% FBS and 1% Pen/Strep. Tachyzoites were harvested and pelleted by centrifugation at 2200g for 10 min and resuspended in prewarmed modified DM or 50:50% (v/v) EMEM and EGM-2MV culture medium before injection into the lumen of the epithelial tubes for infect studies.

### Immunofluorescence staining

For immunostaining, cells were fixed with 4% (v/v) paraformaldehyde (Alfa Aesar) for 20 min and permeabilized with 0.2% (v/v) Triton X-100 (MP Biomedicals) for 10 min with three 1× PBS wash steps between each solution. To reduce nonspecific background fluorescence from collagen, cells were incubated in 0.1 M glycine (Thermo Fisher Scientific, Pittsburgh, PA) for 30 min and washed with 1× PBS three times. Subsequently, cells were blocked with buffer solution [3% (w/v) BSA and 0.1% (v/v) Tween 20 (Thermo Fisher Scientific)] overnight at 4°C. Primary antibodies (table S2) diluted in buffer solution were added to the microdevices and incubated at 4°C for 2 days and washed with 1× PBS three times. Secondary antibodies (table S2) were added to the buffer solution and incubated for 1 day at 4°C. For cytoskeletal actin and nuclear staining, Alexa Fluor-conjugated phalloidin (Thermo Fisher Scientific) and Hoechst 33342 (Thermo Fisher Scientific) at 1:100 were also added to the secondary antibody buffer solution. Lumens were then rinsed with 1× PBS three times over a 2-day period.

### Image acquisition

Bright-field and fluorescent images were captured on a Nikon Ti Eclipse microscope with a top stage incubator equipped with temperature and CO<sub>2</sub> control (set at 37°C and 5%, respectively). Neutrophil kinetic parameters including end-to-end displacement and migration speed were analyzed with Fiji (<https://imagej.net/Fiji>) using the track-mate module. Confocal images were acquired at University of Wisconsin-Madison Optical Imaging Core using a Leica SP8 microscope.

### Optical metabolic imaging

A custom-built inverted multiphoton microscope (Bruker Fluorescence Microscopy, Middleton, WI) was used to acquire fluorescence intensity and lifetime images. The equipment consists of an ultrafast laser (Coherent, Chameleon Ultra II), an inverted microscope (Nikon, Eclipse Ti), and a 40× water immersion (1.15 numerical aperture, Nikon) objective. Fluorescence intensity and lifetime data were collected sequentially with a GaAsP PMT (Hamamatsu, H7422PA-40). FAD fluorescence was isolated using an emission band-pass filter of 550/100 nm and an excitation wavelength of 890 nm. NAD(P)H fluorescence was isolated using an emission band-pass filter of 440/80 nm and an excitation wavelength of 750 nm. The optical redox ratio was determined from the NAD(P)H and FAD lifetime data by integrating the photons detected at each pixel in the image to calculate the total intensity. For each pixel, the intensity of NAD(P)H was then divided by the intensity of FAD. Using Cell Profiler, an automated cell segmentation pipeline was created. This system identified pixels belonging to nuclear regions by using a customized threshold code. Cells were recognized by propagating out from the nuclei within the image. To refine the propagation and to prevent it from continuing into background pixels, an Otsu Global threshold was used. The cell cytoplasm was defined as the cell borders minus the nucleus. Values for NAD(P)H intensity, FAD intensity, and the optical redox ratio [NAD(P)H/FAD intensity] were averaged for all pixels within each cell cytoplasm. At least 100 cells per sample were analyzed, and every experiment was repeated at least three times.

### Cell retrieval from microdevice

To quantify gene expression related to proliferation, differentiation and a function of the intestinal epithelium primary intestinal epithelial

cells were selectively retrieved from the intestinal tissue MPS consisting of epithelial and endothelial tubes. The upper half of the microdevice was removed to expose the collagen hydrogel. The hydrogel was then transferred to an Eppendorf tube containing 300 μl of type I collagenase (6 mg/ml). The sample was incubated on ice for 2 min to degrade the hydrogel and release the cells. Two microliters of biotinylated anti–epithelial cell adhesion molecule (EpCAM) (Thermo Fisher Scientific) was added, and the sample was incubated at 4°C for 15 min. Ten microliters of SeraMAGS beads coupled to streptavidin was added, and the sample was incubated for another 10 min at 4°C. The SeraMAGS beads, with the epithelial cells (EpCAM-positive), were isolated using a magnet and lysed for PCR analysis.

To quantify gene expression related to protective immunity, neutrophils were selectively retrieved from the intestinal tissue MPS 6 hours after introduction into the endothelial vessel. Nonadherent neutrophils were first collected from the endothelial vessels through the pipet-accessible ports (fig. S10). To isolate neutrophils that have migrated into the ECM gel, a 2-mm-diameter biopsy punch (Thermo Fisher Scientific) was used to cut out the hydrogel next to the endothelial vessel. The hydrogel punches were transferred to an Eppendorf tube and digested using collagenase as described above. To separate CD31-positive endothelial cells, Dynabeads CD31 (Thermo Fisher Scientific) endothelial cell depletion was conducted using the manufacturer's guidelines, leaving behind neutrophils in suspension. These neutrophils were mixed with neutrophils collected from the endothelial vessel and lysed for PCR analysis.

### Reverse transcription quantitative polymerase chain reaction

To study how primary intestinal epithelial cells and neutrophils adapted to the microenvironment within the intestinal tissue MPS, the expression of multiple genes related to different pathways was analyzed by RT-qPCR. Briefly, mRNA was isolated from cells using the Dynabeads mRNA DIRECT Purification Kit (Invitrogen). Isolated mRNA was quantified using a Qubit fluorometer (Thermo Fisher Scientific) and the Qubit RNA BR Assay Kit (Thermo Fisher Scientific). Complementary DNA (cDNA) was generated using the High Capacity RNA-to-cDNA Kit (Applied Biosystem) and pre-amplified with SsoAdvanced PreAmp Supermix (Bio-Rad) using primers from Integrated DNA Technologies or Thermo Fisher Scientific (tables S3 and S4). cDNA was analyzed by RT-qPCR using iTaq Universal SYBR Green Supermix (Bio-Rad) or Roche LightCycler master mix according to the manufacturer's protocols in Roche's LightCycler 480 II. Gene expression was normalized using the ΔΔ<sup>Ct</sup> method. To quantify genomic DNA of *T. gondii*, infected epithelial tubes were digested as described above, and genomic DNA was extracted using TRIzol according to the manufacturer's instructions. DNA was purified by phenol/chloroform extraction followed by ethanol precipitation. Genomic DNA was used as the template for preamplification and RT-PCR, as described above, using *T. gondii* primers (table S2).

### Multiplex cytokine/chemokine assays and analysis

To measure NK cell-mediated cytokines secretion, media were collected from intestinal tissue MPS with *T. gondii*-infected epithelium in the presence and absence of NK cells. Media were collected after 24 hours in culture and cytokine/chemokine concentrations analyzed using the Inflammation 20-Plex Human ProcartaPlex panel (EPX200-12185-901, Thermo Fisher Scientific) following the manufacturer's

guidelines. Data were collected on a MAGPIX Luminex xMAP system (Luminex Corporation) using Luminex xPONENT software. Concentration of each analyte was determined from a standard curve, generated by fitting a five-parameter logistic regression of median fluorescence on known concentrations of each analyte.

### Statistical analysis

Data were analyzed (Prism 9.0; GraphPad Software). The normal distribution assumption for statistical tests was confirmed by the Shapiro-Wilk test. Statistical significance was assessed using Student's *t* tests when comparing two conditions/groups, and when comparing more than two groups, significance was assessed using one-way analysis of variance (ANOVA) corrected using the Tukey's test. For nonparametric comparisons, a Mann-Whitney *U* test or a Kruskal-Wallis test was performed.

### SUPPLEMENTARY MATERIALS

Supplementary material for this article is available at <https://science.org/doi/10.1126/sciadv.abm8012>

[View/request a protocol for this paper from Bio-protocol.](#)

### REFERENCE AND NOTES

- D. L. Sacks, Vaccines against tropical parasitic diseases: A persisting answer to a persisting problem. *Nat. Immunol.* **15**, 403–405 (2014).
- J. J. Bigna, J. N. Tochie, D. N. Tounouga, A. O. Bekolo, N. S. Ymelle, E. L. Youda, P. S. Sime, J. R. Nansseu, Global, regional, and country seroprevalence of *Toxoplasma gondii* in pregnant women: A systematic review, modelling and meta-analysis. *Sci. Rep.* **10**, 12102 (2020).
- A. A. Scalise, N. Kakogiannos, F. Zanardi, F. Iannelli, M. Giannotta, The blood–brain and gut–vascular barriers: From the perspective of claudins. *Tissue Barriers* **9**, 1926190 (2021).
- D. Buzoni-Gatel, J. Schulthess, L. C. Menard, L. H. Kasper, Mucosal defences against orally acquired protozoan parasites, emphasis on *Toxoplasma gondii* infections. *Cell. Microbiol.* **8**, 535–544 (2006).
- J. Mestas, C. C. W. Hughes, Of mice and not men: Differences between mouse and human immunology. *J. Immunol.* **172**, 2731–2738 (2004).
- R. Pifer, F. Yarovinsky, Innate responses to *Toxoplasma gondii* in mice and humans. *Trends Parasitol.* **27**, 388–393 (2011).
- W. Ernst, Humanized mice in infectious diseases. *Comp. Immunol. Microbiol. Infect. Dis.* **49**, 29–38 (2016).
- L. D. Shultz, M. A. Brehm, J. V. Garcia-Martinez, D. L. Greiner, Humanized mice for immune system investigation: Progress, promise and challenges. *Nat. Rev. Immunol.* **12**, 786–798 (2012).
- G. Vunjak-Novakovic, K. Ronaldson-Bouchard, M. Radisic, Organs-on-a-chip models for biological research. *Cell* **184**, 4597–4611 (2021).
- L. Si, H. Bai, M. Rodas, W. Cao, C. Y. Oh, A. Jiang, R. Moller, D. Hoagland, K. Oishi, S. Horiochi, S. Uhl, D. Blanco-Melo, R. A. Albrecht, W.-C. Liu, T. Jordan, B. E. Nilsson-Payant, I. Golyntker, J. Frere, J. Logue, R. Haupt, M. McGrath, S. Weston, T. Zhang, R. Plebani, M. Soong, A. Nurani, S. M. Kim, D. Y. Zhu, K. H. Benam, G. Goyal, S. E. Gilpin, R. Prantil-Baum, S. P. Gygi, R. K. Powers, K. E. Carlson, M. Frieman, B. R. tenOever, D. E. Ingber, A human-airway-on-a-chip for the rapid identification of candidate antiviral therapeutics and prophylactics. *Nat. Biomed. Eng.* **5**, 815–829 (2021).
- J. Kim, K.-T. Lee, J. S. Lee, J. Shin, B. Cui, K. Yang, Y. S. Choi, N. Choi, S. H. Lee, J.-H. Lee, Y.-S. Bahn, S.-W. Cho, Fungal brain infection modelled in a human-neurovascular-unit-on-a-chip with a functional blood-brain barrier. *Nat. Biomed. Eng.* **5**, 830–846 (2021).
- A. M. Ortega-Prieto, J. K. Skelton, C. Cherry, M. A. Briones-Orta, C. A. Hateley, M. Dorner, "Liver-on-a-chip" cultures of primary hepatocytes and Kupffer cells for hepatitis B virus infection. *J. Vis. Exp.* 10.3791/58333 (2019).
- S. Jalili-Firoozinezhad, F. S. Gazzaniga, E. L. Calamari, D. M. Camacho, C. W. Fadel, A. Bein, B. Swenor, B. Nestor, M. J. Cronce, A. Tovagliero, O. Levy, K. E. Gregory, D. T. Breact, J. M. S. Cabral, D. L. Kasper, R. Novak, D. E. Ingber, A complex human gut microbiome cultured in an anaerobic intestine-on-a-chip. *Nat. Biomed. Eng.* **3**, 520–531 (2019).
- S. E. Blutt, S. E. Crawford, S. Ramani, W. Y. Zou, M. K. Estes, Engineered human gastrointestinal cultures to study the microbiome and infectious diseases. *Cell. Mol. Gastroenterol. Hepatol.* **5**, 241–251 (2018).
- M. Maurer, M. S. Gresnigt, A. Last, T. Wollny, F. Berlinghof, R. Pospisch, Z. Cseresnyes, A. Medyukhina, K. Graf, M. Gröger, M. Raasch, F. Siwczak, S. Nietzsche, I. D. Jacobsen, M. T. Figge, B. Hube, O. Huber, A. S. Mosig, A three-dimensional immunocompetent intestine-on-chip model as an in vitro platform for functional and microbial interaction studies. *Biomaterials* **220**, 119396 (2019).
- M. Nikolaev, O. Mitrofanova, N. Broguiere, S. Geraldo, D. Dutta, Y. Tabata, B. Elci, N. Brandenberg, I. Kolotuev, N. Gjorevski, H. Clevers, M. P. Lutolf, Homeostatic mini-intestines through scaffold-guided organoid morphogenesis. *Nature* **585**, 574–578 (2020).
- J. A. Brassard, M. Nikolaev, T. Hübscher, M. Hofer, M. P. Lutolf, Recapitulating macro-scale tissue self-organization through organoid bioprinting. *Nat. Mater.* **20**, 22–29 (2021).
- M. Kasendra, A. Tovagliero, A. Sontheimer-Phelps, S. Jalili-Firoozinezhad, A. Bein, A. Chalkiadaki, W. Scholl, C. Zhang, H. Rickner, C. A. Richmond, H. Li, D. T. Breact, D. E. Ingber, Development of a primary human small intestine-on-a-chip using biopsy-derived organoids. *Sci. Rep.* **8**, 2871 (2018).
- D. L. Ivanova, T. M. Mundhenke, J. P. Gigley, The IL-12- and IL-23-dependent NK cell response is essential for protective immunity against secondary *Toxoplasma gondii* infection. *J. Immunol.* **203**, 2944–2958 (2019).
- C. R. Sturge, A. Benson, M. Raetz, C. L. Wilhelm, J. Mirpuri, E. S. Vitetta, F. Yarovinsky, TLR-independent neutrophil-derived IFN-γ is important for host resistance to intracellular pathogens. *Proc. Natl. Acad. Sci. U.S.A.* **110**, 10711–10716 (2013).
- B. Gregg, B. C. Taylor, B. John, E. D. Tait-Wojno, N. M. Grgis, N. Miller, S. Wagage, D. S. Roos, C. A. Hunter, Replication and distribution of *Toxoplasma gondii* in the small intestine after oral infection with tissue cysts. *Infect. Immun.* **81**, 1635–1643 (2013).
- H. Clevers, The intestinal crypt, a prototype stem cell compartment. *Cell* **154**, 274–284 (2013).
- M. E. Gentile, I. L. King, Blood and guts: The intestinal vasculature during health and helminth infection. *PLOS Pathog.* **14**, e1007045 (2018).
- E. J. Jones, T. Korcsmaros, S. R. Carding, Mechanisms and pathways of *Toxoplasma gondii* transepithelial migration. *Tissue Barriers* **5**, e1273865 (2017).
- K. J. Pittman, L. J. Knoll, Long-term relationships: The complicated interplay between the host and the developmental stages of *Toxoplasma gondii* during acute and chronic infections. *Microbiol. Mol. Biol. Rev.* **79**, 387–401 (2015).
- J. L. Coombes, B. A. Charsar, S.-J. Han, J. Halkias, S. W. Chan, A. A. Koshy, B. Striepen, E. A. Robey, Motile invaded neutrophils in the small intestine of *Toxoplasma gondii*-infected mice reveal a potential mechanism for parasite spread. *Proc. Natl. Acad. Sci. U.S.A.* **110**, E1913–E1922 (2013).
- M. Sasai, M. Yamamoto, Innate, adaptive, and cell-autonomous immunity against *Toxoplasma gondii* infection. *Exp. Mol. Med.* **51**, 1–10 (2019).
- J. P. Gigley, The diverse role of NK cells in immunity to *Toxoplasma gondii* infection. *PLOS Pathog.* **12**, e1005396 (2016).
- L. J. Barkal, C. L. Procknow, Y. R. Alvarez-García, M. Niu, J. A. Jiménez-Torres, R. A. Brockman-Schneider, J. E. Gern, L. C. Denlinger, A. B. Theberge, N. P. Keller, E. Berthier, D. J. Beebe, Microbial volatile communication in human organotypic lung models. *Nat. Commun.* **8**, 1770 (2017).
- S. J. Trietsch, E. Naumovska, D. Kurek, M. C. Setyawati, M. K. Vormann, K. J. Wilschut, H. L. Lanz, A. Nicolas, C. P. Ng, J. Joore, S. Kustermann, A. Roth, T. Hankemeier, A. Moisan, P. Vullo, Membrane-free culture and real-time barrier integrity assessment of perfused intestinal epithelium tubes. *Nat. Commun.* **8**, 262 (2017).
- T. Sato, D. E. Stange, M. Ferrante, R. G. J. Vries, J. H. Van Es, S. Van den Brink, W. J. Van Houdt, A. Pronk, J. Van Gorp, P. D. Siersema, H. Clevers, Long-term expansion of epithelial organoids from human colon, adenoma, adenocarcinoma, and Barrett's epithelium. *Gastroenterology* **141**, 1762–1772 (2011).
- M. Fujii, M. Matano, K. Toshimitsu, A. Takano, Y. Mikami, S. Nishikori, S. Sugimoto, T. Sato, Human intestinal organoids maintain self-renewal capacity and cellular diversity in niche-inspired culture condition. *Cell Stem Cell* **23**, 787–793.e6 (2018).
- J. R. Spence, C. N. Mayhew, S. A. Rankin, M. F. Kuhar, J. E. Vallance, K. Tolle, E. E. Hoskins, V. V. Kalinichenko, S. I. Wells, A. M. Zorn, N. F. Shroyer, J. M. Wells, Directed differentiation of human pluripotent stem cells into intestinal tissue in vitro. *Nature* **470**, 105–109 (2011).
- M. Antfolk, K. B. Jensen, A bioengineering perspective on modelling the intestinal epithelial physiology in vitro. *Nat. Commun.* **11**, 6244 (2020).
- N. Gjorevski, N. Sachs, A. Manfrin, S. Giger, M. E. Bragina, P. Ordóñez-Morán, H. Clevers, M. P. Lutolf, Designer matrices for intestinal stem cell and organoid culture. *Nature* **539**, 560–564 (2016).
- Y. Wang, R. Kim, S. S. Hinman, B. Zwarycz, S. T. Magness, N. L. Allbritton, Bioengineered systems and designer matrices that recapitulate the intestinal stem cell niche. *Cell. Mol. Gastroenterol. Hepatol.* **5**, 440–453.e1 (2018).
- L. J. Knoll, T. Tomita, L. M. Weiss, Bradyzoite development, in *Toxoplasma gondii*, L. M. Weiss, K. Kim, Eds. [Academic Press (Elsevier), ed. 2, 2014], pp. 521–549.
- C. R. Sturge, F. Yarovinsky, Complex immune cell interplay in the gamma interferon response during *Toxoplasma gondii* infection. *Infect. Immun.* **82**, 3090–3097 (2014).
- U. Boehm, T. Klamp, M. Groot, J. C. Howard, Cellular responses to interferon-γ. *Annu. Rev. Immunol.* **15**, 749–795 (1997).
- C. Bogdan, M. Röllinghoff, A. Diefenbach, The role of nitric oxide in innate immunity. *Immunol. Rev.* **173**, 17–26 (2000).

41. F. Wang, S. Zhang, R. Jeon, I. Vuckovic, X. Jiang, A. Lerman, C. D. Folmes, P. D. Dzeja, J. Herrmann, Interferon gamma induces reversible metabolic reprogramming of M1 macrophages to sustain cell viability and pro-inflammatory activity. *EBioMedicine* **30**, 303–316 (2018).
42. R. Appelberg, Neutrophils and intracellular pathogens: Beyond phagocytosis and killing. *Trends Microbiol.* **15**, 87–92 (2007).
43. W. Zhao, D. K. Fogg, M. J. Kaplan, A novel image-based quantitative method for the characterization of NETosis. *J. Immunol. Methods* **423**, 104–110 (2015).
44. M. C. Skala, K. M. Riching, A. Gendron-Fitzpatrick, J. Eickhoff, K. W. Elceir, J. G. White, N. Ramanujam, In vivo multiphoton microscopy of NADH and FAD redox states, fluorescence lifetimes, and cellular morphology in precancerous epithelia. *Proc. Natl. Acad. Sci. U.S.A.* **104**, 19494–19499 (2007).
45. R. Datta, A. Gillette, M. Stefely, M. C. Skala, Recent innovations in fluorescence lifetime imaging microscopy for biology and medicine. *J. Biomed. Opt.* **26**, e070603 (2021).
46. N. Courret, S. Darche, P. Sonigo, G. Milon, D. Buzoni-Gatel, I. Tardieu, CD11c- and CD11b-expressing mouse leukocytes transport single *Toxoplasma gondii* tachyzoites to the brain. *Blood* **107**, 309–316 (2006).
47. S. M. Lachenmaier, M. A. Deli, M. Meissner, O. Liesenfeld, Intracellular transport of *Toxoplasma gondii* through the blood-brain barrier. *J. Neuroimmunol.* **232**, 119–130 (2011).
48. Y. Chen, W. Zhou, T. Roh, M. K. Estes, D. L. Kaplan, In vitro enteroid-derived three-dimensional tissue model of human small intestinal epithelium with innate immune responses. *PLOS ONE* **12**, e0187880 (2017).
49. H. Clevers, Modeling development and disease with organoids. *Cell* **165**, 1586–1597 (2016).
50. G. Rossi, A. Manfrin, M. P. Lutolf, Progress and potential in organoid research. *Nat. Rev. Genet.* **19**, 671–687 (2018).
51. H. Derricott, L. Luu, W. Y. Fong, C. S. Hartley, L. J. Johnston, S. D. Armstrong, N. Randle, C. A. Duckworth, B. J. Campbell, J. M. Wastling, J. L. Coombes, Developing a 3D intestinal epithelium model for livestock species. *Cell Tissue Res.* **375**, 409–424 (2019).
52. P. E. Correa Leite, J. de Araujo Portes, M. R. Pereira, F. B. Russo, E. S. Martins-Duarte, N. Almeida dos Santos, M. Attias, F. J. Barrantes, P. C. Baleiro Beltrão-Braga, W. de Souza, Morphological and biochemical repercussions of *Toxoplasma gondii* infection in a 3D human brain neurospheres model. *Brain Behav. Immun. Health* **11**, 100190 (2021).
53. H.-H. Seo, H.-W. Han, S.-E. Lee, S.-H. Hong, S.-H. Cho, S. C. Kim, S. K. Koo, J.-H. Kim, Modelling *Toxoplasma gondii* infection in human cerebral organoids. *Emerg. Microbes Infect.* **9**, 1943–1954 (2020).
54. Y. Wang, M. DiSalvo, D. B. Gunasekara, J. Dutton, A. Proctor, M. S. Lebhar, I. A. Williamson, J. Speer, R. L. Howard, N. M. Smiddy, S. J. Bultman, C. E. Sims, S. T. Magness, N. L. Allbritton, Self-renewing monolayer of primary colonic or rectal epithelial cells. *Cell. Mol. Gastroenterol. Hepatol.* **4**, 165–182.e7 (2017).
55. D. Holthaus, E. Delgado-Betcourt, T. Aebsicher, F. Seeber, C. Klotz, Harmonization of protocols for multi-species organoid platforms to study the intestinal biology of *Toxoplasma gondii* and other protozoan infections. *Front. Cell. Infect. Microbiol.* **10**, 610368 (2021).
56. G. Altay, E. Larrañaga, S. Tosi, F. M. Barriga, E. Batlle, V. Fernández-Majada, E. Martínez, Self-organized intestinal epithelial monolayers in crypt and villus-like domains show effective barrier function. *Sci. Rep.* **9**, 10140 (2019).
57. N. Barker, Adult intestinal stem cells: Critical drivers of epithelial homeostasis and regeneration. *Nat. Rev. Mol. Cell Biol.* **15**, 19–33 (2013).
58. E. Y. Denkers, A. G. Schneider, S. B. Cohen, B. A. Butcher, Phagocyte responses to protozoan infection and how *Toxoplasma gondii* meets the challenge. *PLOS Pathog.* **8**, e1002794 (2012).
59. S. K. Bliss, L. C. Gavrilescu, A. Alcaraz, E. Y. Denkers, Neutrophil depletion during *Toxoplasma gondii* infection leads to impaired immunity and lethal systemic pathology. *Infect. Immun.* **69**, 4898–4905 (2001).
60. T. S. Lima, S. Mallya, A. Jankeel, I. Messaoudi, M. B. Lodoen, *Toxoplasma gondii* extends the life span of infected human neutrophils by inducing cytosolic PCNA and blocking activation of apoptotic caspases. *MBio* **12**, e02031–20 (2021).
61. S. Varikuti, B. K. Jha, G. Volpedo, N. M. Ryan, G. Halsey, O. M. Hamza, B. S. McGwire, A. R. Satoskar, Host-directed drug therapies for neglected tropical diseases caused by protozoan parasites. *Front. Microbiol.* **9**, 2655 (2018).
62. T. M. Scharton-Kersten, T. A. Wynn, E. Y. Denkers, S. Bala, E. Grunvald, S. Hieny, R. T. Gazzinelli, A. Sher, In the absence of endogenous IFN- $\gamma$ , mice develop unimpaired IL-12 responses to *Toxoplasma gondii* while failing to control acute infection. *J. Immunol.* **157**, 4045–4054 (1996).
63. A. J. Lee, A. A. Ashkar, The dual nature of type I and type II interferons. *Front. Immunol.* **9**, 2061 (2018).
64. F. J. D. Mennechet, L. H. Kasper, N. Rachinel, W. Li, A. Vandewalle, D. Buzoni-Gatel, Lamina propria CD4+ T lymphocytes synergize with murine intestinal epithelial cells to enhance proinflammatory response against an intracellular pathogen. *J. Immunol.* **168**, 2988–2996 (2002).
65. P. M. Robben, M. LaRegina, W. A. Kuziel, L. D. Sibley, Recruitment of Gr-1+ monocytes is essential for control of acute toxoplasmosis. *J. Exp. Med.* **201**, 1761–1769 (2005).
66. B. Villeret, L. Brault, A. Couturier-Maillard, P. Robinet, V. Vasseur, T. Secher, I. Dimier-Poisson, M. Jacobs, S.-G. Zheng, V. F. Quesniaux, B. Ryffel, Blockade of IL-1R signaling diminishes Paneth cell depletion and *Toxoplasma gondii* induced ileitis in mice. *Am. J. Clin. Exp. Immunol.* **2**, 107–116 (2013).
67. S. J. Melchor, C. M. Saunders, I. Sanders, J. A. Hatter, K. A. Byrnes, S. Coutermash-Ott, S. E. Ewald, IL-1R regulates disease tolerance and cachexia in *Toxoplasma gondii* infection. *J. Immunol.* **204**, 3329–3338 (2020).
68. J. Y. Channon, K. A. Miselis, L. A. Minns, C. Dutta, L. H. Kasper, *Toxoplasma gondii* induces granulocyte colony-stimulating factor and granulocyte-macrophage colony-stimulating factor secretion by human fibroblasts: Implications for neutrophil apoptosis. *Infect. Immun.* **70**, 6048–6057 (2002).
69. H. Jebbari, C. W. Roberts, D. J. Ferguson, H. Bluethmann, J. Alexander, A protective role for IL-6 during early infection with *Toxoplasma gondii*. *Parasite Immunol.* **20**, 231–239 (1998).
70. M. Rostami Nejad, S. J. Sherafat, M. Roshani, M. Telkabadi, F. Lahmi, K. Cheraghipour, A. R. Kaboli, M. Alavi-Moghaddam, The evaluation of interleukin-8 chemokine in chronic and acute *Toxoplasma gondii* infection. *Gastroenterol. Hepatol. Bed Bench* **4**, 34–37 (2011).
71. G. Perona-Wright, K. Mohrs, F. M. Szabla, L. W. Kummer, R. Madan, C. L. Karp, L. L. Johnson, S. T. Smiley, M. Mohrs, Systemic but not local infections elicit immunosuppressive IL-10 production by natural killer cells. *Cell Host Microbe* **6**, 503–512 (2009).
72. A. K. R. Kwaa, C. A. G. Talana, J. N. Blankson, Interferon- $\alpha$  enhances NK cell function and the suppressive capacity of HIV-specific CD8 $^{+}$  T cells. *J. Virol.* **93**, e01541–18 (2019).
73. M. N. Kelly, J. K. Kolls, K. Happel, J. D. Schwartzman, P. Schwarzenberger, C. Combe, M. Moretto, I. A. Khan, Interleukin-17/Interleukin-17 receptor-mediated signaling is important for generation of an optimal morphomorphonuclear response against *Toxoplasma gondii* infection. *Infect. Immun.* **73**, 617–621 (2005).
74. I. A. Khan, J. A. MacLean, F. S. Lee, L. Casciotti, E. DeHaan, J. D. Schwartzman, A. D. Luster, IP-10 is critical for effector T cell trafficking and host survival in *Toxoplasma gondii* infection. *Immunity* **12**, 483–494 (2000).
75. B. Spellberg, J. E. Edwards Jr., Type 1/type 2 immunity in infectious diseases. *Clin. Infect. Dis.* **32**, 76–102 (2001).
76. T. Kiniwa, Y. Enomoto, N. Terazawa, A. Omi, N. Miyata, K. Ishiwata, A. Miyajima, NK cells activated by Interleukin-4 in cooperation with Interleukin-15 exhibit distinctive characteristics. *Proc. Natl. Acad. Sci. U.S.A.* **113**, 10139–10144 (2016).
77. D. L. Ivanova, R. Krempels, S. L. Denton, K. D. Fettell, G. M. Saltz, D. Rach, R. Fatima, T. Mundhenke, J. Materi, I. R. Dunay, J. P. Gigley, NK Cells negatively regulate CD8 T Cells to promote immune exhaustion and chronic *Toxoplasma gondii* infection. *Front. Cell. Infect. Microbiol.* **10**, 313 (2020).
78. M. M. Mahe, N. Sundaram, C. L. Watson, N. F. Shroyer, M. A. Helmrath, Establishment of human epithelial enteroids and colonoids from whole tissue and biopsy. *J. Vis. Exp.* **97**, 52483 (2015).
79. K. L. VanDussen, N. M. Sonnek, T. S. Stappenbeck, L-WRN conditioned medium for gastrointestinal epithelial stem cell culture shows replicable batch-to-batch activity levels across multiple research teams. *Stem Cell Res.* **37**, 101430 (2019).
80. M. Karlsson, C. Zhang, L. Méar, W. Zhong, A. Digre, B. Katona, E. Sjöstedt, L. Butler, J. Odeberg, P. Dusart, F. Edfors, P. Oksvold, K. von Feilitzen, M. Zwahlen, M. Arif, O. Altay, X. Li, M. Ozcan, A. Mardinoglu, L. Fagerberg, J. Mulder, Y. Luo, F. Ponten, M. Uhlen, C. Lindskog, A single-cell type transcriptomics map of human tissues. *Sci. Adv.* **7**, eabh2169 (2021).

**Acknowledgments:** We acknowledge BioRender.com for aid in creating Figs. 1A, 2, A and B, 3A, 4Ai, 5Ai, and 6Ai. We thank E. Carchman from the Department of Surgery and UWCCC Biobank at University of Wisconsin-Madison (UW-Madison) for the supply of small intestinal tissue and Huttenlocher Lab from the Department of Medical Microbiology and Immunology at UW-Madison for facilitating blood draws from healthy donors. We also thank the UW Optical Imaging Core for the support on the 3D confocal imaging. **Funding:** This work was funded by the NIH grant F31CA247248 (to M.H.), NIH grant R01CA186134, NIH grant R01AI144016, and University of Wisconsin Carbone Cancer Center Support Grant NIH P30CA014520. **Author contributions:** M.H., J.M.A., K.Y.P., M.C.S., S.C.K., L.J.K., and D.J.B. conceptualized and designed the research. M.H. performed experiments and did data analysis with assistance from J.M.A., K.Y.P., and B.M.D.G. M.H., J.M.A. S.C.K., L.J.K., and D.J.B. wrote the manuscript. All authors reviewed the manuscript. **Competing interests:** D.J.B. holds equity in Bellbrook Labs LLC, Tasso Inc., Salus Discovery LLC, Lynx Biosciences Inc., Stacks to the Future LLC, Turba LLC, Flambeau Diagnostics LLC, and Onexio Biosystems LLC. D.J.B. is also a consultant for Abbott Laboratories. The authors declare that they have no other competing interests. **Data and materials availability:** All data needed to evaluate the conclusions in the paper are present in the paper and/or the Supplementary Materials.

Submitted 29 October 2021

Accepted 23 March 2022

Published 6 May 2022

10.1126/sciadv.eabm8012